

## Evaluation of the Use of Homogenized Fuel Assemblies in the Thermal Analysis of Spent Fuel Storage Casks

G.R. Thomas  
R.W. Carlson

July 1999



This is an informal report intended primarily for internal or limited external distribution. The opinions and conclusions stated are those of the author and may or may not be those of the Laboratory.

Work performed under the auspices of the Department of Energy by the Lawrence Livermore National Laboratory under Contract W-7405-Eng-48.

#### DISCLAIMER

This document was prepared as an account of work sponsored by an agency of the United States Government. Neither the United States Government nor the University of California nor any of their employees, makes any warranty, express or implied, or assumes any legal liability or responsibility for the accuracy, completeness, or usefulness of any information, apparatus, product, or process disclosed, or represents that its use would not infringe privately owned rights. Reference herein to any specific commercial product, process, or service by trade name, trademark, manufacturer, or otherwise, does not necessarily constitute or imply its endorsement, recommendation, or favoring by the United States Government or the University of California. The views and opinions of authors expressed herein do not necessarily state or reflect those of the United States Government or the University of California, and shall not be used for advertising or product endorsement purposes.

This report has been reproduced  
directly from the best available copy.

Available to DOE and DOE contractors from the  
Office of Scientific and Technical Information  
P.O. Box 62, Oak Ridge, TN 37831  
Prices available from (423) 576-8401

Available to the public from the  
National Technical Information Service  
U.S. Department of Commerce  
5285 Port Royal Rd.,  
Springfield, VA 22161

---

---

# **Evaluation of the Use of Homogenized Fuel Assemblies in the Thermal Analysis of Spent Fuel Storage Casks**

---

---

**Prepared by  
G. R. Thomas  
R. W. Carlson**

**Prepared for  
U.S. Nuclear Regulatory Commission  
Office of Nuclear Material Safety and Safeguards**



**FESSP**

**Fission Energy and Systems Safety Program**

**Lawrence Livermore National Laboratory**

### Disclaimer

This document was prepared as an account of work sponsored by an agency of the United States Government. Neither the United States Government nor the University of California, nor any of their employees, makes any warranty, express or implied, or assumes any legal liability or responsibility for the accuracy, completeness, or usefulness of any information, apparatus, product, or process disclosed, or represents that its use would not infringe privately owned rights. Reference herein to any specific commercial product, process, or service by trade name, trademark, manufacturer, or otherwise, does not necessarily constitute or imply its endorsement, recommendation, or favoring by the United States Government or the University of California. The views and opinions of authors expressed herein do not necessarily state or reflect those of the United States Government or the University of California and shall not be used for advertising or product endorsement purposes.

This work was supported by the United States Nuclear Regulatory Commission under a Memorandum of Understanding with the United States Department of Energy, and performed under the auspices of the U.S. Department of Energy by Lawrence Livermore National Laboratory under Contract W-7405-Eng-48.

---

---

# **Evaluation of the use of Homogenized Fuel Assemblies in the Thermal Analysis of Spent Fuel Storage Casks**

---

---

**Manuscript date: May 5, 1999**

**Prepared by  
G. R. Thomas  
R. W. Carlson**

**Lawrence Livermore National Laboratory  
7000 East Avenue  
Livermore, CA 94550**

**Prepared for  
U.S. Nuclear Regulatory Commission  
Office of Nuclear Material Safety and Safeguards**



## **ABSTRACT**

Thermal analysis of spent fuel storage casks has generally been based on the assumption that heat released by the fuel assemblies is transported to the cask cavity only by conduction through the walls of the basket. This conservative assumption was adopted to compensate for uncertainties in modeling heat transfer in the cavity of a spent fuel cask. During recent years, some applicants have submitted safety analysis reports for spent fuel storage casks that challenge this assumption. They offer two methods which include the fuel assemblies, as well as the walls of the basket, as part of the path for heat transfer to the cask cavity. A third method, the consideration of a fuel assembly as a homogeneous "log," is explored in a study described in this report.



# CONTENTS

<b>1. Introduction</b>	<b>1</b>
Method 1: Model Each Fuel Rod in the Fuel Assembly	1
Method 2: Determine an Effective Thermal Conductivity	1
Concerns with These Methods	1
A New Method: Consider Fuel Assemblies as Homogeneous "Logs"	2
<b>2.0 Heat Transfer in Spent Nuclear Fuel Assemblies</b>	<b>3</b>
2.1 Heat Generation in the Fuel	4
2.2 Radiation Heat Transfer	4
Emissivity	4
View Factor	5
Attenuation of Radiation	5
2.3 Convection Heat Transfer	5
Surface Characteristics	6
2.4 Conduction Heat Transfer	6
Conduction through the Cladding	7
2.5 Summary	7
<b>3.0 Experimental Data Set Selection and Description</b>	<b>9</b>
3.1 Selection of the Fuel Temperature Tests	9
3.2 Description of the Fuel Temperature Tests	9
3.2.1 Description of the Fuel Temperature Test Apparatus	9
3.2.2 Fuel Temperature Test Temperature Measurements	14
3.2.3 Control of the Fuel Temperature Test Boundary Conditions	14
3.2.4 Thermal Modeling Considerations of the Fuel Temperature Test Apparatus	16
3.3 Use of the FTT Experimental Data Sets	17
3.3.1 Fuel Temperature Test Apparatus Symmetry	17
3.3.2 Fuel Temperature Test Data Reduction	17
3.3.3 Use of the Fuel Temperature Test Data in this Study	18
3.3.4 Determination of Axially Local Fuel Temperature Test Canister Temperatures	18
<b>4.0 Thermal Models Used in Simulating FTT Experimental Data Sets</b>	<b>19</b>
4.1 Thermal Modeling Tools	19
4.2 Thermal Models Used in Simulating the FTT Experimental Data Sets	19
4.2.1 Thermal Model for Simulating the Fuel Temperature Test at Vacuum Conditions	19
4.2.2 Thermal Model for Simulating the Fuel Temperature Test for Helium-filled and Air-Filled Conditions	21
<b>5.0 Results of the Simulation of the FTT Experiments</b>	<b>27</b>
5.1 Approach to Thermal Modeling of the FTT Experiments	27
5.2 Thermal Modeling of the FTT Experiments at Vacuum Conditions	27
5.3 Thermal Modeling of the FTT Experiments with Helium and Air Conditions	28
5.4 Quantitative Comparison of the FTT Experiments to TOPAZ3D Results	32
5.4.1 Temperature Comparisons	32
5.4.2 Effective Thermal Conductivity Results	32
5.4.3 Temperature at Thermocouple Level 7	32
5.5 Quantitative Comparison of Results to the Manteufel and Todreas Study	34

<b>6.0 Conclusions</b> .....	<b>37</b>
<b>7.0 References</b> .....	<b>39</b>
<b>Appendix A: Fuel Temperature Test Data and primary data reduction</b> .....	<b>41</b>

## FIGURES

Figure 1. Pressurized water reactor fuel assembly (Masche 1971; Viebrock 1981) .....	3
Figure 2. Perspective cutaway view of the FTT apparatus (Bates 1986, Figure 3-1).....	10
Figure 3. Fuel assembly support cage (Bates 1986, Figure 3-5) .....	11
Figure 4. Fuel assembly canister (Bates 1986, Figure 3-4).....	12
Figure 5. Test stand (Bates 1986, Figure 3-4).....	13
Figure 6. Closure lid assembly (Bates 1986, Figure 3-6) .....	15
Figure 7. Test stand cross section (Bates 1986, Figure 3-3).....	16
Figure 8. Canister lid thremowell identification (Bates 1986, Figure 3-7) .....	18
Figure 9. FTT axial power shape with annotations (Bates 1986, Figure 3-11).....	20
Figure 10. Perspective view of the TOPAZ3D thermal model of the FTT geometry with the fuel assembly replaced by a solid square log looking towards the center line .....	22
Figure 11. Perspective view of the TOPAZ3D thermal model of the FTT geometry with the fuel assembly replaced by a solid square log with outer gas region removed looking radially outward.....	23
Figure 12. Perspective view of the solid log looking towards the centerline .....	24
Figure 13. Perspective view of the five internal vertical regions in the solid square log which represent the FTT temperature locations looking towards the centerline .....	25
Figure 14. TOPAZ3D versus actual FTT data: helium and air test diagonal temperature distributions at TC level 3.....	29
Figure 15. TOPAZ3D versus actual FTT data: helium and air test diagonal temperature distributions at TC level 4.....	30
Figure 16. TOPAZ3D versus actual FTT data: helium and air test diagonal temperature distributions at TC level 5.....	31

## **ACKNOWLEDGMENT**

This work was funded by the Spent Fuel Project Office, U. S. Nuclear Regulatory Commission (NRC). The authors would like to thank Steven Hogsett, technical monitor in the Spent Fuel Technical Review Section at the NRC, for his overall direction and specific contributions. The timely response and attention to detail by Lyssa Campbell during preparation of the manuscript are greatly appreciated.



# EVALUATION OF THE USE OF HOMOGENIZED FUEL ASSEMBLIES IN THE THERMAL ANALYSIS OF SPENT FUEL STORAGE CASKS

## 1. INTRODUCTION

Thermal analysis of spent fuel storage casks has generally been based on the assumption that heat released by the fuel assemblies is transported to the cask cavity only by conduction through the walls of the basket. This conservative assumption was adopted to compensate for uncertainties in modeling heat transfer in the cavity of a spent fuel cask. During recent years, some applicants have submitted safety analysis reports for spent fuel storage casks that challenge this assumption. They offer two methods (described below) which include the fuel assemblies, as well as the walls of the basket, as part of the path for heat transfer to the cask cavity. A third method, the consideration of a fuel assembly as a homogeneous "log," is explored in this report.

### **Method 1: Model Each Fuel Rod in the Fuel Assembly**

The first method attempts to model each fuel rod in every fuel assembly of a symmetrical section of the basket. Radiation heat transfer, combined with conduction through the fill gas and fuel rods, is evaluated to determine the temperatures of all fuel rods in the cask. This extensive analysis was benchmarked by comparison to a test performed at Idaho National Engineering and Environmental Laboratory (INEEL), where instrumented spent fuel assemblies were inserted into spent fuel casks purchased from cask vendors.

### **Method 2: Determine an Effective Thermal Conductivity**

To simplify the analytical modeling, the second approach utilizes an effective thermal conductivity to represent homogenized fuel assemblies. The effective thermal conductivity is determined by requiring agreement between measurement and calculation for one of the tests performed at INEEL using instrumented spent fuel assemblies in a controlled simulated storage cask environment.

The lack of detail in the model employed for this approach places substantial importance on the benchmarking to provide assurance that the effective thermal conductivity accurately approximates the combined radiation, convection, and conduction heat transfer within the fuel assembly.

### **Concerns with These Methods**

While the two methods include fuel assemblies as part of the heat transfer path to the cask cavity, this is only one portion of the entire thermal analysis of a spent fuel storage cask. If conservatism is reduced in this portion of the analysis, an evaluation of the uncertainties in the remainder of the analysis should be completed to assure that the final result does not become non-conservative. For example, the uncertainty in the heat transfer between the basket periphery and the cask wall is a complicated combination of radiation, convection, and conduction. This heat transfer, which can be sufficiently difficult to predict, requires conservatism in the modeling of heat transfer in the basket to assure conservatism in the prediction of peak fuel rod temperature.

It is important to note that the INEEL experiments included only measurements of the temperatures in the guide tubes and the temperature of the environment. There were no measurements of the temperature of the basket or the surface of the cask body; therefore, calculations of these intermediate temperatures cannot be benchmarked against experimental data.

## **A New Method: Consider Fuel Assemblies as Homogeneous “Logs”**

Due to the limitations of the first two methods, another option was implemented to evaluate models that consider the fuel assemblies homogeneous “logs” with uniform thermal conductivity and internal heat generation. This study was directed to test the feasibility of using a solid log with a constant thermal conductivity to replace each fuel assembly in a spent fuel transportation-storage cask.

The study initially involved a review of several existing experimental programs dealing with the heat transfer characteristics of both spent fuel assemblies and the integral system of spent fuel transportation-storage casks of varying designs (Bates 1986; Creer 1986; Creer 1987; Cuta 1986; McKinnon 1987; McKinnon 1989; Strobe 1990; Cuta and Creer 1986). The purpose of this review was to select what would appear to be the best experimental data that would provide a basis for testing the solid log concept. This selected experimental data set then would be evaluated with a thorough thermal analysis involving, at the core, a detailed thermal model of the experimental apparatus and the surrounding environment that would affect experimental results. This thermal model would include replacement of any fuel assemblies involved in the experimental data set with solid logs.

This model is to be compared with as many different benchmark experiments as possible to assure that the unique characteristics of one experiment do not give rise to biased results, leading to a less conservative boundary of results for all types of fuel assemblies in all types of casks.

Based upon the results, the reported effective thermal conductivities can be used with a model that represents the fuel assemblies as a homogenous log to determine the heat transfer across fuel assemblies.

## 2.0 HEAT TRANSFER IN SPENT NUCLEAR FUEL ASSEMBLIES

Heat transfer in a spent nuclear fuel assembly is a complicated combination of conduction, convection, and radiation that defies prediction from first principals because the geometry and material properties are, at best, poorly known. The geometry of a fuel assembly is shown in Figure 1. The fuel rods have been omitted from this figure to emphasize the location and configuration of the spacers and guide tubes. Ultimately, the consideration of heat transfer across a fuel assembly reduces to heat transfer from one fuel rod to neighboring fuel rods. The terms that must be considered in fuel assembly heat transfer include the generation of heat in the fuel as well as radiation, convection, and conduction heat transfer. Each term will be addressed in the following paragraphs with emphasis on factors impacting each of the modes of heat transfer. There is no effort to combine the effects of the modes of heat transfer in a fuel assembly in this chapter.

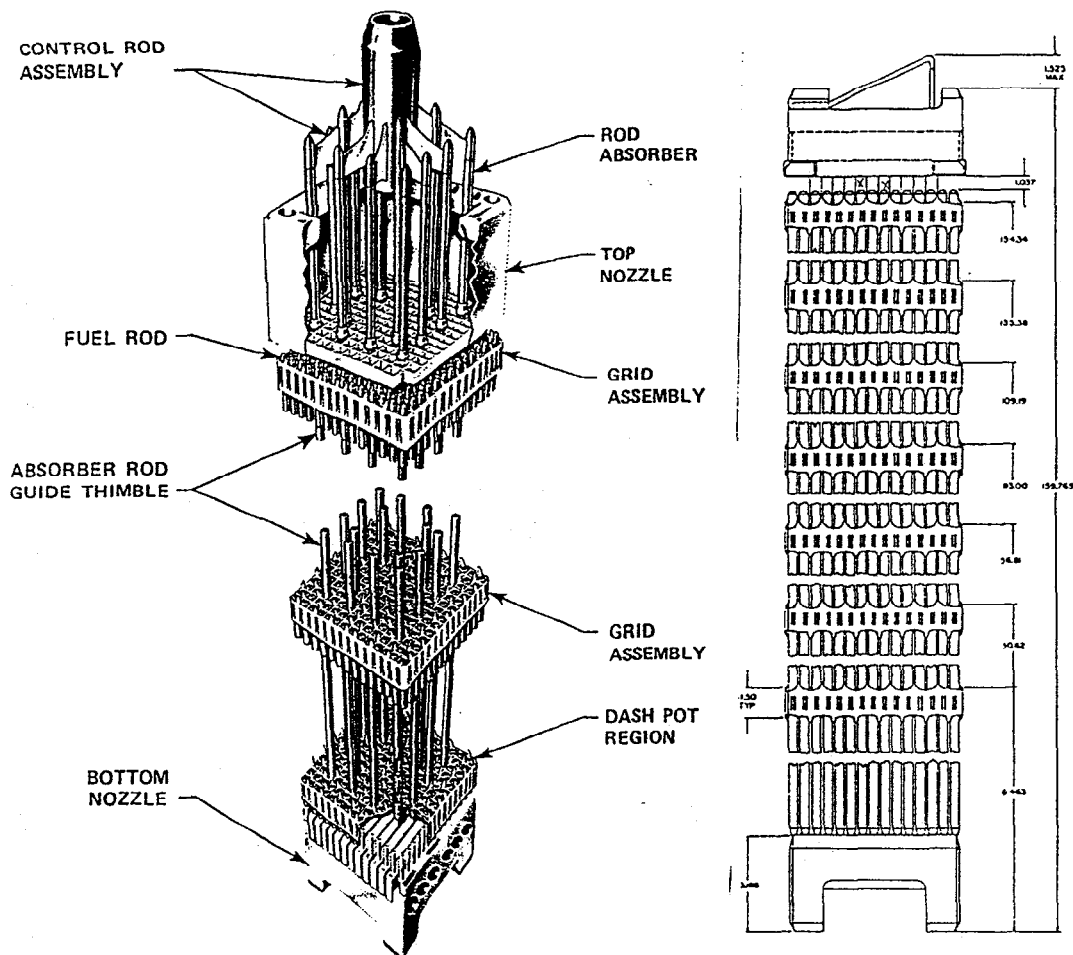


Figure 1. Pressurized water reactor fuel assembly (Masche 1971; Viebrock 1981)

## 2.1 Heat Generation in the Fuel

While the fuel assembly is in the reactor, the interaction of the neutrons with the uranium produces either fissions or parasitic neutron captures in the uranium or in the other materials in the reactor. The fission process results in fission product isotopes, which are radioactive, decaying by emission of gamma rays, beta, and alpha particles. The neutron captures in the uranium or other materials produce radioactive activation products. The attenuation of the radiation emitted by these isotopes ultimately results in increased motion of the molecules which becomes deposited heat. When the reactor is initially shut down, the heat produced by the radioactive decay is about 10% of the heat produced when the reactor was in operation. After residing for 5 to 10 years in the spent fuel pool of the reactor, the heat produced is reduced to a fraction of one percent of the heat released when the reactor was in operation. Heat production rates from 1 to 1.5 kW/MTU are typical at the start of storage. The axial distribution of the heat production rate typically results in an axial peaking factor of about 1.1 with regions about one foot long at the ends of the fuel assembly where the heat production rate is less than the average.

Because  $UO_2$  is an excellent shield material, most of the radiation emitted from the fuel at the center of a fuel assembly will be absorbed by the fuel rods at the periphery of that fuel assembly. This is also true for all fuel assemblies in a spent fuel storage or transport cask. Consequently, there will be a small and gradual increase in the amount of heat released from the fuel rods toward the outside of the array. There will also be a slight increase in the heat production rate near the guide tubes due to the absence of uranium to absorb the radiation in the guide tubes. These variations are expected to amount to a few percent difference between the maximum and minimum heat production rates within the array of fuel assemblies.

## 2.2 Radiation Heat Transfer

The dominant mode of heat transfer between irradiated fuel rods is thermal radiation. The radiation heat transfer is non-uniform because it occurs between a unit area on one fuel rod and any unit area of any other fuel rod. Both the temperature and surface conditions vary from fuel rod to fuel rod.

The expression that quantifies radiative heat transfer is:

$$q'_i = \sum_{j=1}^N A_j \mathcal{F}_{i-j} \sigma (T_i^4 - T_j^4)$$

and

$$\mathcal{F}_{i-j} = \frac{1}{\frac{1}{F_{i-j}} + \left( \frac{1}{\epsilon_i} - 1 \right) + \frac{A_i}{A_j} \left( \frac{1}{\epsilon_j} - 1 \right)}$$

The primary variables in this expression are the surface emissivity ( $\epsilon_i$ ,  $\epsilon_j$ ) of the fuel rods, the view factor ( $F_{i-j}$ ) between elements of the fuel rods, and any attenuation of the radiant energy transfer by the fill gas which is not included in this expression. Each of these will be addressed in the following paragraphs.

### Emissivity

During irradiation, the cladding can absorb oxygen from the water, forming an oxide layer on its outer surface. Simultaneously, deposits of various materials in the water can be deposited on the outer surface, forming a layer that is referred to as crud. The composition, tenacity, and surface

characteristics of the crud layer are primarily governed by the water chemistry. This can vary from reactor to reactor, from fuel cycle to fuel cycle within a reactor, and even from fuel rod to fuel rod within a fuel assembly. Consequently, the emissivity of the surface is not a well-defined parameter, and measurements of the surface emissivity are not necessarily universally applicable.

The equation above assumes isotropic emission of radiation that should be appropriate if the surface of the crud is uniformly rough. However, if patches of the crud have flaked off, or if scratches in the crud layer have developed during removal of a fuel assembly from the reactor core, or from insertion of the fuel assembly into the spent fuel storage rack or into the spent fuel storage cask, the radiation will not be isotropic.

### **View Factor**

The view factor can be computed by dividing the surface of each fuel rod into many small surface elements and computing the view factor between a surface element on one fuel rod and the surface elements on the other fuel rods. While this calculation is time consuming, it is possible.

The use of a single view factor to represent the heat transfer from one entire fuel rod to adjacent fuel rods is inappropriate because the fuel rod temperature varies circumferentially and axially. Any attempt to use such a model should be accompanied by an analysis demonstrating that the variation in temperature is sufficiently small to have no impact upon the computed heat transfer rate. The axial variation in temperature and view factor is created by the spacers which effectively fill the region between the fuel rods while providing a metallic pathway for heat transfer between fuel rods.

### **Attenuation of Radiation**

The gas that fills the region between the fuel rods can absorb a portion of the radiation much like a cloud (water vapor) absorbs a portion of the radiant energy that reaches the surface of the earth. This phenomenon is typically small if the fill gas is monatomic or diatomic. However, if the gas molecule has three or more atoms such as  $\text{H}_2\text{O}$  or  $\text{CO}_2$ , the attenuation can be very significant. The attenuation of radiation is a non-uniform function of the wavelength of the radiation. Calculation of the attenuation requires treating the gas as a participating member in the exchange of radiant energy that both absorbs energy and emits energy to achieve equilibrium.

## **2.3 Convection Heat Transfer**

The presence of a fill gas permits transfer of heat from the surface of the cladding by a moving boundary layer while a quiescent zone occupies the remainder of the region between fuel rods. Characterizing the convection heat transfer is complicated by the presence of spacers that maintain the geometry of the fuel rods. When the fuel assembly is in the reactor, the spacers serve to mix the coolant as it flows upward through the fuel assembly. Fins are incorporated into the spacer that cause the mixing and, during storage in a spent fuel cask, these fins will interfere with the boundary layers that are the essence of natural circulation. At the least, the fins will cause the natural circulation to transition to turbulent and at the worst, the fins will inhibit the movement of the fill gas and eliminate natural circulation as a heat transfer mechanism.

The correlation for convection heat transfer from a flat vertical plate to the adjacent boundary layer is (Churchill and Chu 1975):

$$Nu = \left[ 0.825 + \frac{0.387Ra^{1/6}}{\left[ 1 + \left( \frac{0.492}{Pr} \right)^{9/16} \right]^{8/27}} \right]^2$$

where

$$Nu = \frac{hL}{k}$$

$$Ra = GrPr = \frac{g\beta(T_s - T_\infty)L^3}{\nu\alpha}$$

$$Pr = \frac{c_p\mu}{k}$$

This correlation is valid for vertical flow over flat plates and may be extended to vertical flow over cylinders (fuel rods) of height  $L$  if the boundary layer thickness  $\delta$  is much less than the diameter  $D$  of the cylinder. Satisfaction of this requirement is assured by satisfying the following condition (Sparrow and Gregg 1956):

$$\frac{D}{L} \geq \frac{35}{Gr^{1/4}}$$

However, some empirical data for slender vertical cylinders satisfies the above condition where the curvature of the surface enhances the heat transfer rate relative to the values predicted by the above correlation.

Satisfying the above condition on the size of the boundary layer also assures that the boundary layer is small compared to the spacing between fuel rods (pitch/diameter =  $14.3/10.7 = 1.334$ ). This assures that the boundary layers from adjacent fuel rods will not interfere with each other and invalidate the correlation based upon unimpeded development of the boundary layer.

### Surface Characteristics

The correlation cited above is based upon experiments that employed a smooth surface with a uniform temperature or uniform heat flux. However, the fuel rods have a non-uniform coating of crud over their surface and the temperature is non-uniform due to variations in the heat transfer rate. As noted in the discussion of radiant heat transfer, patches of crud that are missing or scratches in the crud will interfere with the development of the boundary layer and invalidate the predictions of heat transfer from the correlation for natural convection.

## 2.4 Conduction Heat Transfer

Conduction can be a significant form of heat transfer in two areas. The first is conduction through the gas that fills the region between fuel rods and the second is circumferential conduction of heat within the cladding. Heat absorbed on one side of the cladding must be conducted to the other side so it can be radiated to adjacent fuel rods.

Conduction through the fill gas is important only if convection is insignificant. When convection is significant, a boundary layer develops on the heated surface that flows upward and a boundary layer develops on the cooler surface that flows downward. Between these boundary layers is a

quiescent region where the fill gas has a very small velocity and essentially constant temperature. Since the temperature in the quiescent zone is constant, there is no temperature gradient to support conduction through the gas. However, if the boundary layer formation is inhibited, the fill gas will be a continuous, nearly stationary, medium between the fuel rods. Conduction through the gas will occur while convection will not contribute to the heat transfer.

### **Conduction through the Cladding**

Conduction of heat through the cladding couples the radiant energy entering the fuel rod cladding and the radiant energy leaving the cladding. The metallic portions of the cladding will dominate the conduction of heat in the circumferential direction. The crud layer on the outer surface of the cladding restricts the flow of heat from the Zircaloy to the outer surface of the crud where radiation and convection can transfer the heat to adjacent fuel rods. In addition, the fuel and cladding frequently come into contact during irradiation which adds a parallel conduction path through the fuel.

If the gap between the fuel and the cladding is intact, the fuel will not enter into the circumferential conduction heat transfer and the heat transfer will be a two-region calculation including the cladding and crud. However, if the gap between the fuel and cladding has collapsed, the circumferential conduction heat transfer will be at least a three-region calculation, in which the fuel also enters into the analyses. The characterization of the fuel is further complicated by the fact that zirconium is an oxygen scavenger and will extract oxygen from the uranium dioxide, leaving an oxygen-depleted region at the surface of the fuel. Clearly, removing oxygen from the fuel transforms the fuel toward the metallic state and increases the thermal conductivity of the fuel. However, the thickness of this oxygen-depleted region and the thermal conductivity of this region are not well known and can be expected to vary from fuel rod to fuel rod depending on parameters such as burnup, power distribution, fill gas pressure, and fission product gas release rates. This is further complicated if the fuel rod develops any pinhole leaks, which deplete the gases inside the fuel rods and may permit introduction of water into the interior of the fuel rod.

All these issues are superimposed upon the concern that there is very little measured data to characterize the thermal conductivity of Zircaloy at the conclusion of irradiation. Utilizing the thermal conductivity of unirradiated Zircaloy over-estimates the conduction heat transfer because it ignores the formation of voids during irradiation.

## **2.5 Summary**

The heat transfer modes that should be included in the consideration of fuel assembly heat transfer have been addressed above. The generation of heat in the fuel as well as radiation, convection and conduction heat transfer modes that remove the heat from the assemblies to the storage cask were described. The uncertainty of the values of the material properties that contribute to the specific mode of heat transfer will determine the size of the bounding limits for the mode of heat transfer. There is no effort to combine the effects of the modes and their bounding limits of heat transfer in a fuel assembly in this chapter.

Because of the size of the bounding limits, any attempt to include the fuel assemblies in a spent fuel cask as a reliable heat transfer path should be based upon either a detailed evaluation of each heat transfer mode or a detailed evaluation of the parameters (described above). Alternatively, methods for predicting the heat transfer rate can be carefully benchmarked to experiments that include temperature measurements of both the fuel rods and the materials surrounding the fuel rods. The remainder of this document addresses procedures for benchmarking a method that assumes that a fuel rod can be approximated as a mass with a temperature-dependent thermal conductivity.



## **3.0 EXPERIMENTAL DATA SET SELECTION AND DESCRIPTION**

### **3.1 Selection of the Fuel Temperature Tests**

Available data characterizing the fuel rod temperature distribution in a spent fuel storage cask indicates that the Fuel Temperature Tests [FTT] (Bates 1986) provide the best opportunity to test the concept that characterizes the fuel assemblies as a homogenized medium with constant properties. The primary reasons for this are the ability of the FTT experiments to provide both a sufficiently detailed experimental data base of the temperature distribution throughout a spent fuel assembly and a well-controlled and defined boundary condition. Other test programs (Creer 1986-1; Creer 1986-2; Creer 1987; Cuta 1986; McKinnon 1987; McKinnon 1989; and Strobe 1990) did not provide sufficient data to characterize the fuel rod temperatures without having to estimate parameters significant to the fuel rod temperatures.

The FTT test apparatus used a single spent fuel assembly. The fuel assembly was a Westinghouse-design PWR 15 X 15 array fuel assembly that had been discharged from the Turkey Point Unit 3 reactor. During the FTT experiments, this fuel assembly was generating a decay heat power of about 1.17 kW, which is relatively high for stored spent fuel assemblies. A more typical value of decay heat for spent fuel assemblies starting long-term dry storage (> 5 years after discharge) would probably be 0.5 to 1.0 kW.

The FTT series of tests was selected because it:

- 1) involved identical steady-state tests performed under vacuum conditions and with fill gases of both air and helium (one test each) at reasonable temperature ranges;
- 2) involved more than 100 temperature measurements within the active fuel region of a real spent fuel assembly;
- 3) was located in a well characterized and instrumented apparatus having well-defined and controlled boundary conditions;
- 4) had a relatively high decay power level.

The latter reason, the relatively high decay power, makes use of the solid log replacement concept—an even greater challenge since there will be a greater temperature drop across the spent fuel assembly.

### **3.2 Description of the Fuel Temperature Tests**

#### **3.2.1 Description of the Fuel Temperature Test Apparatus**

Figure 2 shows a cut-away perspective view of the FTT experiment.

In the FTT apparatus, the test fuel assembly was mounted in a strong-back Fuel Assembly Support Cage (Figure 3). The cage provided a base for and continuous axial support of the installed test fuel assembly by relatively large (2 × 2-inch) angle brackets located at all four corners of the test fuel assembly. In addition, there were five horizontal straps located every 76.2 cm over the test fuel assembly length. The assembled Fuel Assembly Support Cage and test fuel assembly were placed inside a large stainless steel canister (Figure 4), which was then placed inside a temperature-controlled and heated Test Stand Liner. This liner, which acts as a guard heater during the FTT experiments, is in turn inserted into an Insulation Sheath — thus forming the Test Stand (Figure 5).

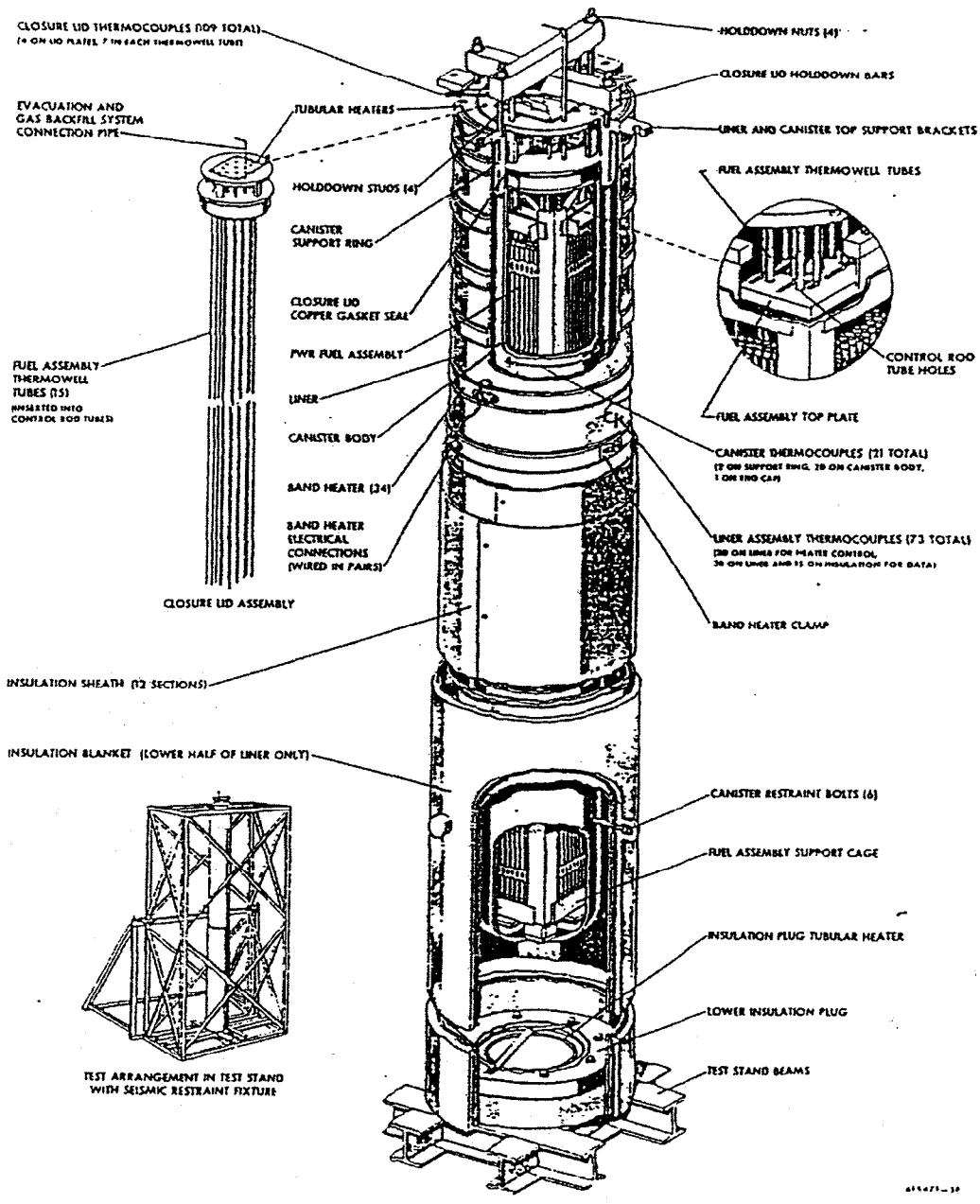


Figure 2. Perspective cutaway view of the FTT apparatus (Bates 1986, Figure 3-1)

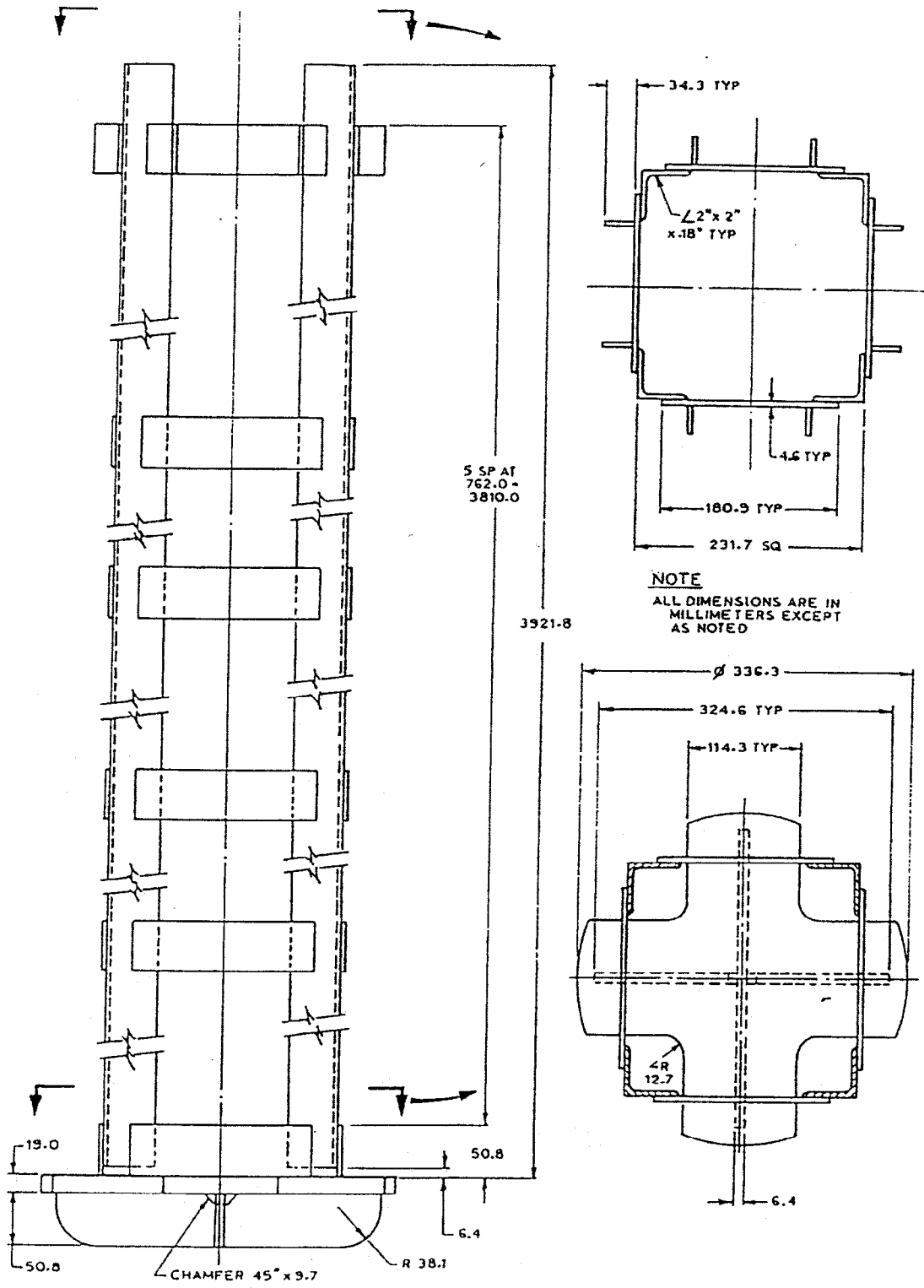
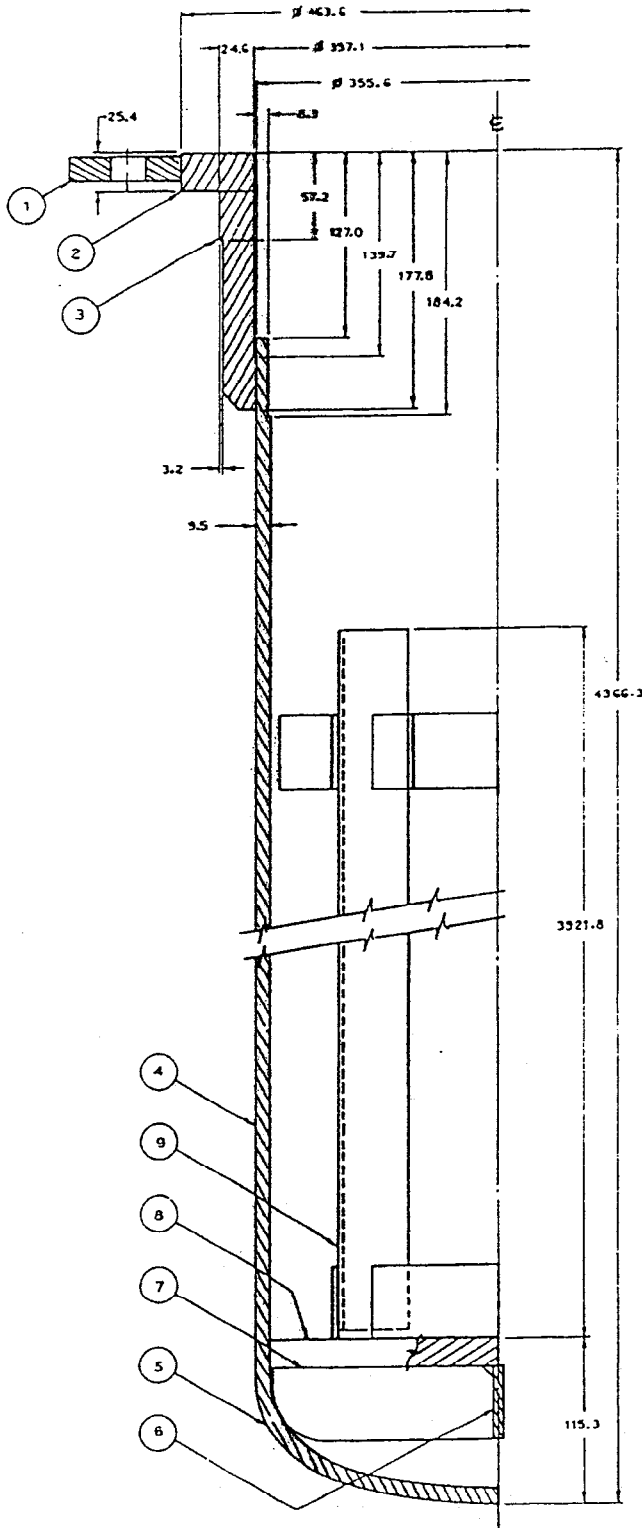


Figure 3. Fuel assembly support cage (Bates 1986, Figure 3-5)



PKNO	QTY	DESCRIPTION	MATERIAL
1	4	CANNISTER TO LINER MOUNTING BRACKET	CARBON STEEL
2	1	TOP PLATE	
3	1	UPPER SUPPORT	304 SST
4	1	CANNISTER BODY 14" SCHED 30 PIPE	
5	1	CANNISTER BODY END CAP 14" SCHED 30	
6	2	SUPPORT WEB	
7	1	SUPPORT WEB	
8	1	BOTTOM CRUCIFORM PLATE	
9	1	FUEL ASSEMBLY SUPPORT FRAME	

**NOTE**  
ALL DIMENSIONS ARE IN MILLIMETERS EXCEPT AS NOTED

Figure 4. Fuel assembly canister (Bates 1986, Figure 3-4)

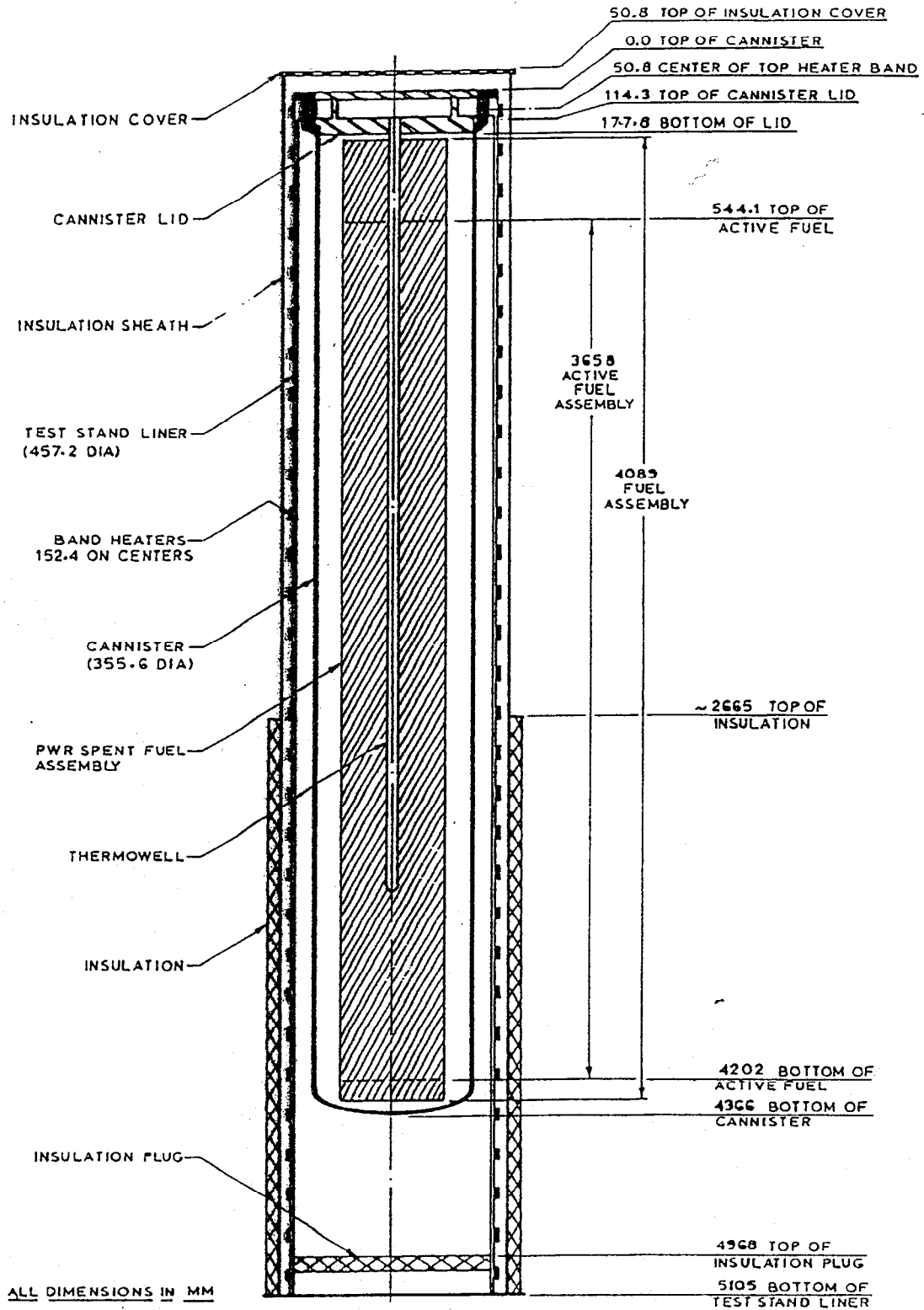


Figure 5. Test stand (Bates 1986, Figure 3-4)

### **3.2.2 Fuel Temperature Test Temperature Measurements**

Thermocouples (TCs) were inserted into the test fuel assembly at fifteen radial locations at each of seven axial locations over the active fuel length for a total of 105 TCs within the test fuel assembly (one, at level five from the bottom, is dedicated to heater control). These TCs were inserted into the test fuel assembly via a Closure Lid Assembly (Figure 6) which contains thermowells that fill the central instrumentation tube and 14 empty control rod guide tubes of the test fuel assembly. The selected positions of the thermowells are shown in both Figures 9 and 10. The latter also presents a good view of the cross-sectional arrangement of the FTT apparatus.

An additional 20 TCs are mounted at five axial locations on the outer surface of the Canister. None of these five locations are coincidental with the test fuel assembly TC locations; however, they do extend from below the bottom-most to above the top-most test fuel assembly axial TC locations.

### **3.2.3 Control of the Fuel Temperature Test Boundary Conditions**

In addition to the extensive TC instrumentation within the test fuel assembly and on the canister surface, one of the major strengths of this FTT apparatus (and unique among the reviewed set of experiments) is the effective control and characterization of the local experimental boundary conditions. The canister containing the test fuel assembly is effectively insulated from the surrounding outside environmental effects. The response of the canister wall to the temperature-controlled heating (by the test fuel assembly TC noted above) from the Test Stand Liner is to establish an azimuthally uniform temperature at any axial level with only a relatively small axial gradient of about 20°C over the length of the active fuel column. The schematic drawing of the Test Stand shown in Figure 5, and the cross-sectional arrangement shown in Figure 7, display the test arrangement that makes this control possible.

The practical result of this test arrangement is that the test fuel assembly defines its own axial and radial temperature gradients, based on conductive-convective-radiative exchange with the isolated and well-defined environment of the surrounding canister that has a locally azimuthally uniform (nearly isothermal) temperature field.

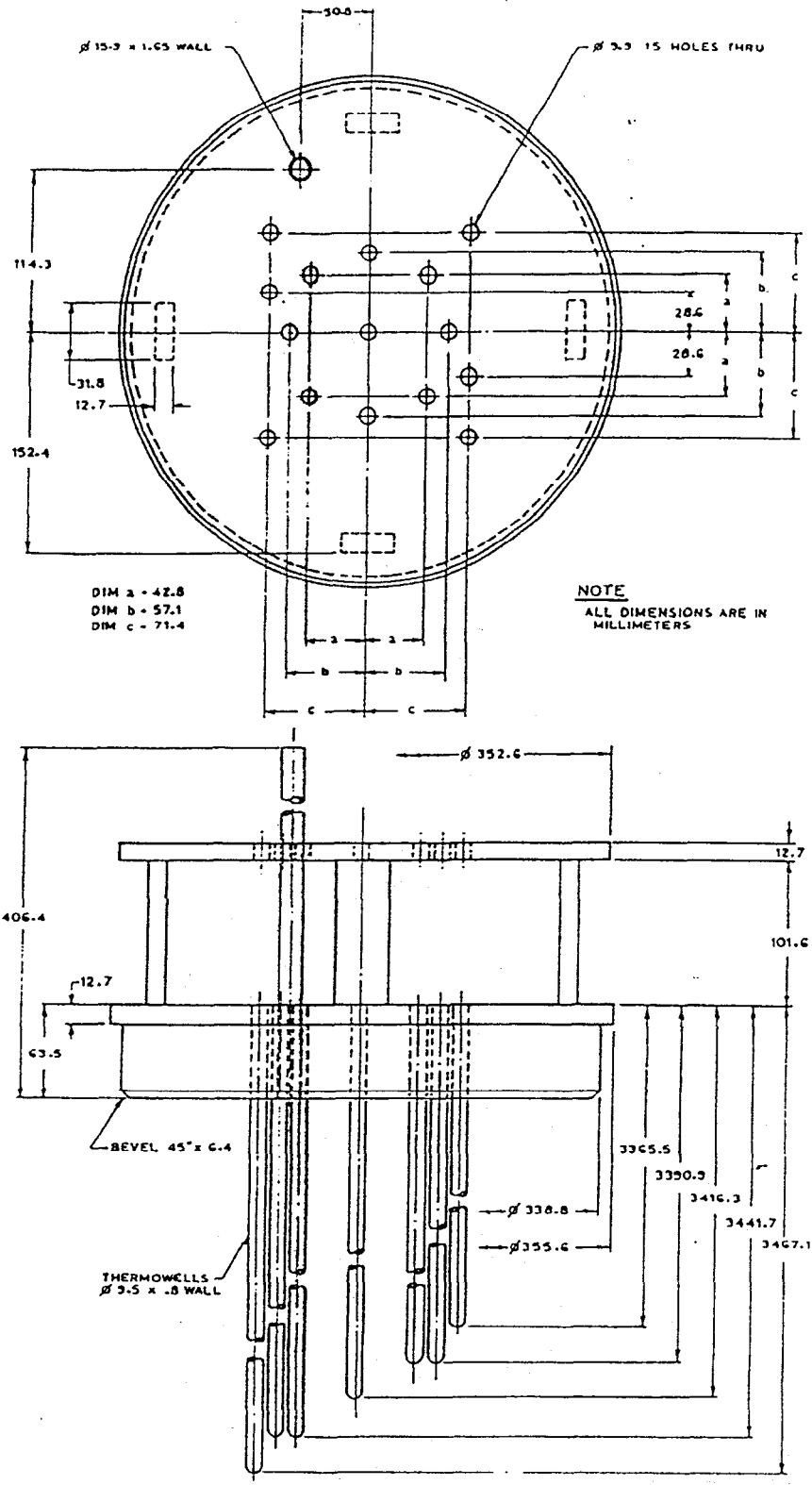


Figure 6. Closure lid assembly (Bates 1986, Figure 3-6)

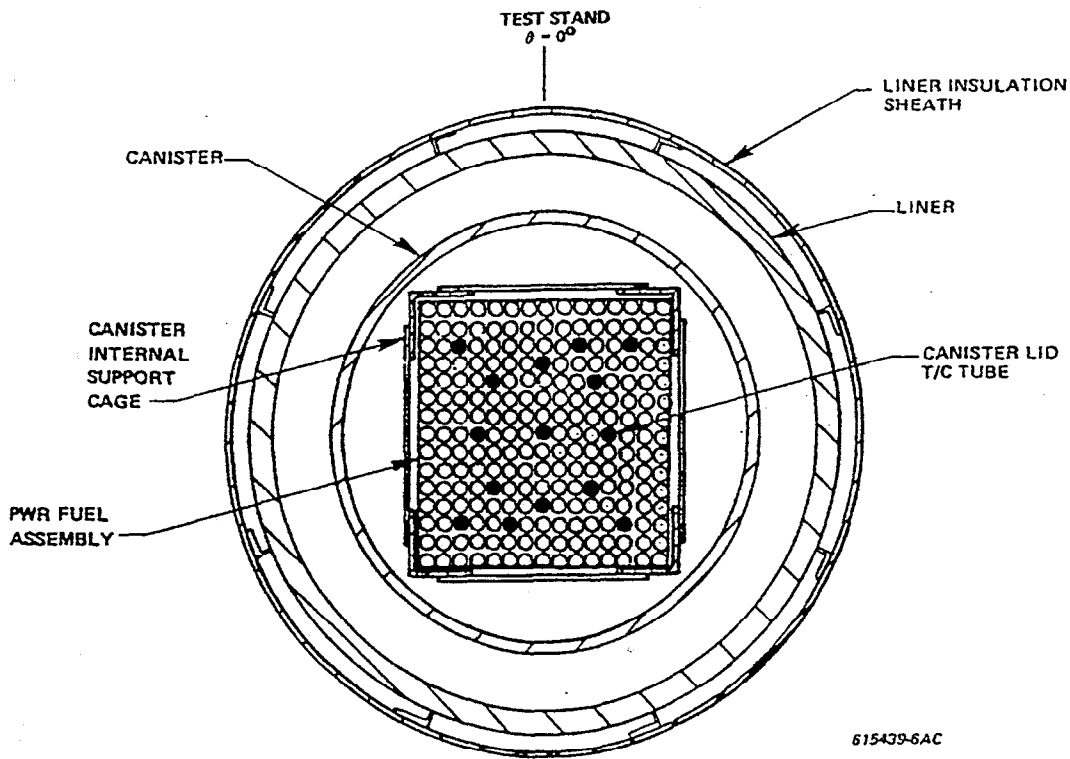


Figure 7. Test stand cross section (Bates 1986, Figure 3-3)

### 3.2.4 Thermal Modeling Considerations of the Fuel Temperature Test Apparatus

At a minimum, to be able to thermally model radially and axially local conditions in the FTT experiments, it is necessary to incorporate essentially all details shown in Figure 7. For example, the full-length  $2 \times 2$ -inch angle brackets at all four corners of the test fuel assembly act as effective radiative shields protecting a substantial portion of the test fuel assembly from directly seeing the canister wall. Also, both these angle brackets and the five horizontal straps located every 76.2 cm over the test fuel assembly length should locally affect both convective and radiative energy exchanges. As a result, a detailed axial and radial thermal modeling of the FTT experimental set must include a modeling of the Fuel Assembly Support Cage.

Similarly, egg-crate-style grid spacers are included in the design of any fuel assembly; typically, seven grid spacers are located axially over the length of a PWR fuel assembly. As would be the case for the horizontal straps of the Fuel Assembly Support Cage, these grid spacers will locally affect energy exchange modes and pathways. A detailed axial and radial thermal modeling of the FTT experimental set (and, in fact, any complete thermal modeling of a fuel assembly) should include a modeling of the presence and effects of the grid spacers.

As described below, this study modeled, in detail, the radial impact of the corner angle brackets of the Fuel Assembly Support Cage, but the possible effects of either the horizontal straps or grid spacers were not studied. That is, the thermal models generated for this study essentially reproduced the FTT cross section shown in Figure 7 minus the Fuel Assembly Support Cage horizontal straps. In Section 5 of this report, there is some discussion of locally anomalous TC readings that might be due to the presence of straps and the test fuel assembly grid spacers.

### 3.3 Use of the FTT Experimental Data Sets

#### 3.3.1 Fuel Temperature Test Apparatus Symmetry

The thermal modeling in this study took advantage of the one-eighth symmetry of the FTT test geometry to fully represent all local test fuel assembly and FTT apparatus geometries.

Similarly, the selection of test fuel assembly internal TC locations has an almost complete one-eighth symmetry as seen in Figure 8. From this figure, it can be seen that there are two complete corner-to-corner diagonal sets of five each TCs (TC sets 2-5-1-11-15 and 4-7-1-10-13) and two complete sets of three each TCs (TC sets 6-1-12 and 9-1-8) perpendicular to the midpoint of the sides of the test fuel assembly. The only non-symmetrical aspect of the TC arrangement is missing pairs of positions corresponding to the symmetry of TCs 3 and 14. As an additional and, for data use, practical view of the TC locations, the TCs can be grouped in the following five symmetrical groups:

- 1) TC 1 (test fuel assembly center)
- 2) TCs 7-11-10-5 (test fuel assembly inner diagonal)
- 3) TCs 4-15-13-2 (test fuel assembly outer diagonal)
- 4) TCs 6-9-12-8 (test fuel assembly perpendicular mid-row)
- 5) TCs 3-14 (test fuel assembly off-set mid-row)

The aspect of test symmetry also applies partially to the 20 TCs located at five axial levels on the outer surface of the canister wall. As noted above, the axial position of these 20 TCs spans the test fuel assembly axial TC locations. The 20 TCs are arranged in axial alignment at 45° spacing starting with the 0° orientation shown in Figure 8, which also aligns them with test fuel assembly TC groupings. However, at the most, no more than four of these TCs are aligned at any single angular orientation.

#### 3.3.2 Fuel Temperature Test Data Reduction

Generally speaking, at any one of the seven axial TC levels, the variation in measured temperatures within each of the symmetric TC groupings 2 through 5 (defined above) was less than about  $\pm 3$  °C. Similarly, at any one of the five canister axial TC levels, the general variation in temperature was about the same or less.

As a result of the consistency of results at symmetrical locations at each axial level, the first step in making use of the FTT data was to average the data based on symmetric TC grouping 2 through 5. Appendix A presents a summary of the data for the three FTT experiments (vacuum, helium, and air). The appendix includes some initial data reduction such as the 2 through 5 group average temperatures.

Referring to Appendix A under the column titled "Ave. Temp," the first three averaged sets of temperatures (both in °F and K) at each axial level represent the test fuel assembly diagonal conditions, or groups 1, 2 and 3 from above (i.e., centerline-inner diagonal-outer diagonal regions [TC 1, TCs 7-11-10-5 and TCs 4-15-13-2]). In this same "Ave. Temp" column, the next number represents group 4 or TCs 6-9-12-8 at the test fuel assembly perpendicular mid-row; the following number, group 5 or TCs 3-14, are at the test fuel assembly off-set mid-row.

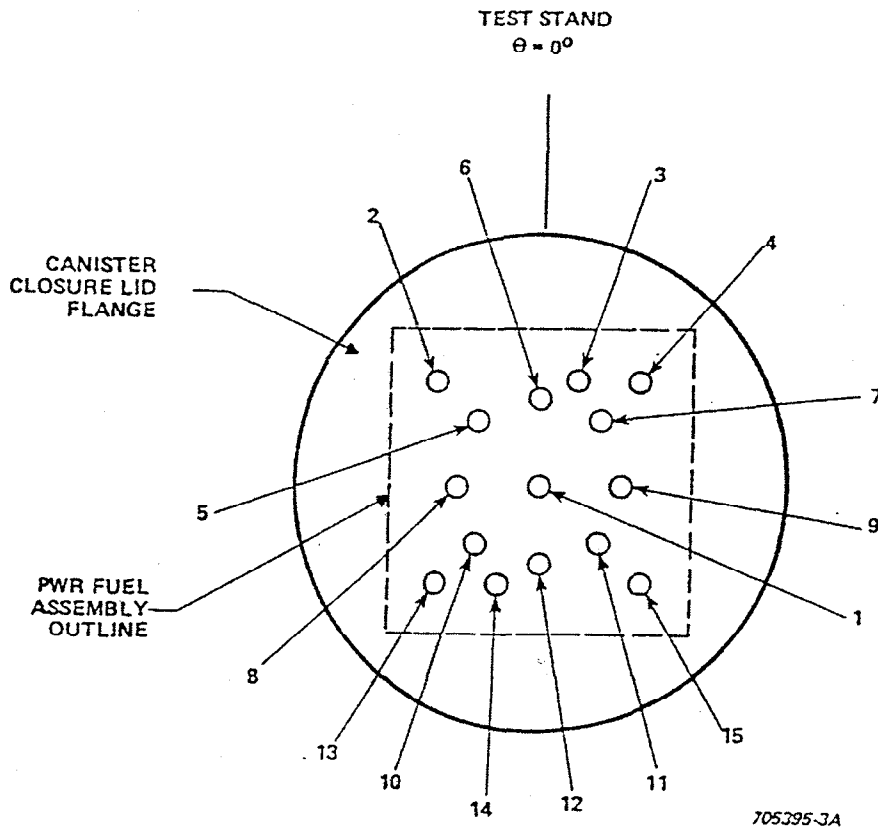


Figure 8. Canister lid thermowell identification (Bates 1986, Figure 3-7)

### 3.3.3 Use of the Fuel Temperature Test Data in this Study

The above four regionally averaged temperatures, plus the centerline temperature, were used in the detailed thermal modeling described in the following section. These temperatures form the basis for evaluating the accuracy of the calculated temperatures for the same five physical locations — in the vacuum test, at the actual modeled locations of the test fuel assembly instrumentation and guide tubes; and in the helium and air tests, at the same five locations within the replacement solid logs.

The interpolated canister wall temperature, described below, provided both a sixth benchmark temperature and the closure boundary condition essential to completing the comparison between the detailed thermal modeling and the FTT temperature data at each axial level for each test.

### 3.3.4 Determination of Axially Local Fuel Temperature Test Canister Temperatures

The final temperature at each axial level in this same column, entered in the third column as TC number 500, represents a calculated equivalent average canister (“Can Wall” at a radius of 7 inches) temperature for that test at that specific axial position. The smooth and well-behaved axial temperature profiles resulting from plots of the azimuthally averaged canister temperatures (also reported under the “Ave. Temp” column) permitted effective interpolation of the canister surface temperature via curve fits. The TC number 500 nodal temperatures were generated using 4th-order curve fits. These same calculated canister temperatures are used in the thermal modeling described below to represent the effectively isothermal boundary conditions for each of the seven axial TC levels in each of the three tests.

## **4.0 THERMAL MODELS USED IN SIMULATING FTT EXPERIMENTAL DATA SETS**

### **4.1 Thermal Modeling Tools**

The primary thermal modeling tool used in this study for simulating the FTT experiments was the TOPAZ3D three-dimensional finite-element heat transfer code (Shapiro 1985). This code, developed at the Lawrence Livermore National Laboratory (LLNL), has been widely used to solve complex steady-state or transient conductive-convective-radiative heat transfer problems.

The strength of the TOPAZ3D code lies in its ability to evaluate conductive-radiative heat transfer with temperature-dependent thermal properties for virtually any conditions in any configuration. The code also can handle convective heat transfer as boundary conditions; but it does not handle flow fields — e.g., the code cannot handle, on first principles, all of the convective effects that would be present in the FTT helium and air tests. However, at a given axial location, the practical effects of convective heat transfer between the test fuel assembly and the balance of the FTT apparatus can be simulated by treating the problem as two-dimensional and adjusting thermal properties of the intervening gas.

To be able to facilitate thermal modeling with the TOPAZ3D code requires two other codes. The first is the INGRID code (Stillman 1985), a generalized geometry-generating code that can create any desired three-dimensional finite-element geometry in the form of a directly usable input file for the TOPAZ3D code. The second is the MONT3D code (Maltby and Burns 1993) to generate a complete radiative exchange factor file for all possible surfaces that can interchange radiative energy, regardless of the complexity of the studied configuration. The MONT3D code uses the same INGRID input deck as required to generate the TOPAZ3D input file with user-supplied radiative emissivity values for each potential radiating surface and Monte Carlo techniques to generate the complete radiative exchange factor file. This radiative exchange factor file is, in the binary form, a direct input file to the TOPAZ3D code.

### **4.2 Thermal Models Used in Simulating the FTT Experimental Data Sets**

#### **4.2.1 Thermal Model for Simulating the Fuel Temperature Test at Vacuum Conditions**

TOPAZ3D code thermal models of the FTT apparatus were generated for analyzing the FTT tests in the form of a detailed one-eighth-symmetry model of the cross section of the FTT apparatus. These models included the fuel assembly with specific representations of the five symmetric locations where FTT temperatures were measured at each axial level. The model also included a symmetric side of one angle bracket, part of the Fuel Assembly Support Cage (Figure 3). It did not include the axially local horizontal straps that are part of that assembly. Thus, the model reproduced the experimental cross section seen in Figure 8 except for the horizontal straps. The outer boundary of this model was a 45° segment of the canister wall.

Although these models were three-dimensional, all analyses in this study are effectively two-dimensional. Three-dimensional TOPAZ3D models of a two-dimensional problem are generated as easily as two-dimensional models. Three-dimensional TOPAZ3D models have the added advantage of being able to bring in the third dimension in the event that it proves necessary to include that dimension — e.g., if it was necessary to study the Fuel Assembly Support Cage horizontal straps and/or test fuel assembly grid spacers.

Decay heat in these models was simulated by selecting a single value (essentially a constant power density) such that the modeled fuel assembly sum was equivalent to that needed to simulate the total axially local decay heat. The axial power shape used throughout this study to determine local power factors corresponding to the seven test fuel assembly TC levels is shown in Figure 9. Figure 9 was taken directly from the FTT report (Bates 1986) with hand-written notations by the authors showing the scaled locations and relative power factors used in this study.

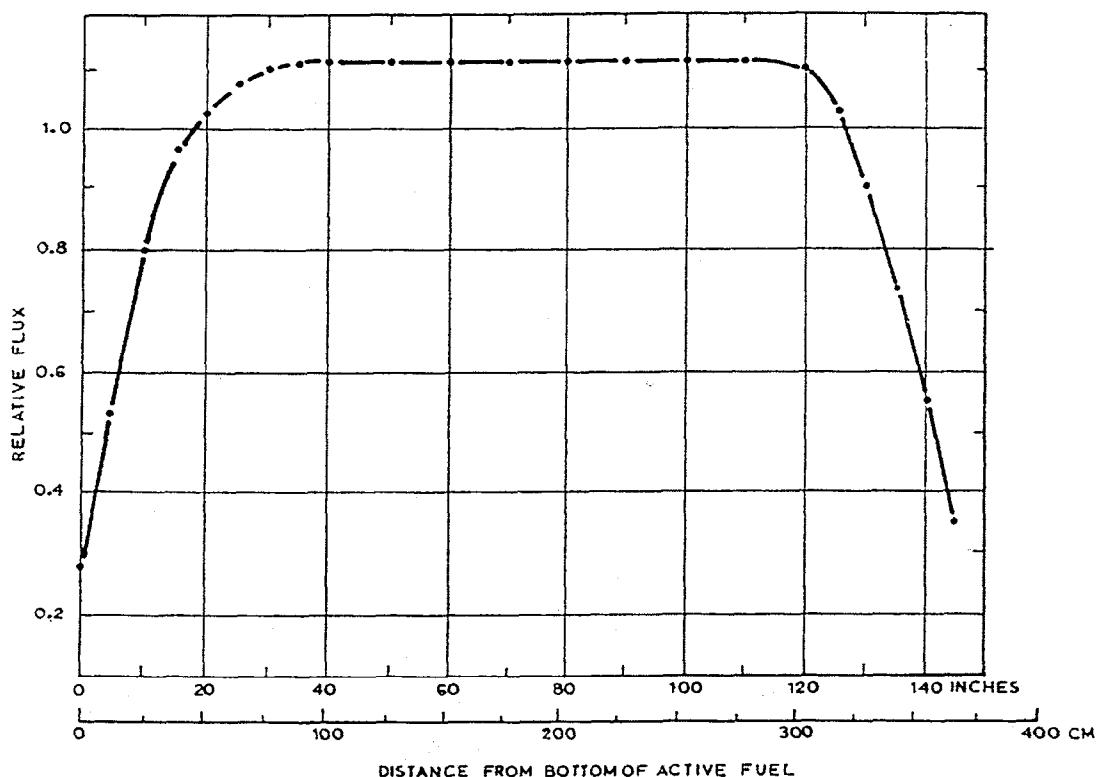


**Figure 9. FTT axial power shape with annotations (Bates 1986, Figure 3-11)**

The first use of the TOPAZ3D model was to study the FTT vacuum test. The primary objective was to match the measured FTT temperatures. In addition, a second objective was to try to determine the effective emissivity of the canister wall inner surface for use throughout this study.

Both objectives were accomplished by matching the measured four regionally averaged guide tube temperatures plus the centrally located instrumentation tube temperature to the calculated temperatures for the same five physical locations in the test fuel assembly. At the same time, it was necessary to coincidentally match the sixth experimental temperature condition imposed by the averaged local canister wall temperatures. These wall temperatures were determined from interpolation of local canister wall temperatures from curve fits at each of the seven axial TC levels in the test fuel assembly and for each of the three tests.

The sixth condition, matching the local canister wall temperature, was an imposed boundary condition in all applications of the TOPAZ3D thermal models in this study. To do this, the canister wall was assigned a constant test and axial level specific temperature (discussed above).

In order to study the effective emissivity of the canister wall inner surface, it was necessary to generate radiative exchange factor files for TOPAZ3D thermal models using the MONT3D code (Maltby and Burns 1993). The files were generated progressively in an iterative fashion while honing in on the best-fit effective emissivity of the canister wall inner surface, as discussed below in the Results section.

Once the objectives were set, the best-fit effective emissivity of the canister wall inner surface was used as input to the companion solid-log thermal model used to study the helium- and air-filled FTT experiments (described below).

#### **4.2.2 Thermal Model for Simulating the Fuel Temperature Test for Helium-filled and Air-Filled Conditions**

After the vacuum test study, the TOPAZ3D code thermal model was modified. The gas-filled region between the solid log replacement for the fuel assembly and both the angle bracket and the canister wall, was filled with an imaginary material. The initial value for thermal conductivity of this material was based on either helium or air as appropriate for the test being studied.

The need for this imaginary material relates to the need to simulate the effective local (at a specific axial level) contribution of the gas convective contribution to the combined convective-radiative heat transfer. The gas convective contribution establishes the relationship between the temperature of the fuel assembly boundary (the replacement solid log) and the angle bracket and canister wall of the FTT test section. The radiative heat transfer among these components was properly accounted for in each of the TOPAZ3D runs. However, because TOPAZ3D does not fully model convective heat transfer, the thermal conductivity of this material would be adjusted between iterative TOPAZ3D runs to simulate the convective heat transfer contribution.

This TOPAZ3D thermal model is shown in perspective views in Figures 10 through 13. In Figure 10, the entire 45° segment, including the imaginary material filling the gas spaces, is shown as if the viewer is outside looking towards the center of the FTT test section. The closest surface to the viewer is the outer surface of the canister wall. In Figure 11, the imaginary material filling the gas spaces has been removed and the perspective has shifted to a viewer position near the center line of the FTT test section looking outward. The three primary components of the model can be seen: the 45° segment of the square log, one half of an angle bracket, and the canister wall.

The 45° segment of the square log has been isolated in Figure 12 (the viewer is again outside, as in Figure 10). By removing the major portion of the square log, the centrally located instrumentation tube and the four off-center guide tube locations in this model (the FTT temperature measurement locations) can be seen in Figure 13 as vertical sections in the solid log. Each of the vertical sections shown in Figure 13 are at the correct location and occupy the same effective volume as the actual instrumentation tube and four appropriate guide tubes. (The TOPAZ3D code output directly produces the local volume-weighted average temperature for each of these volumes.) Using this approach provided a convenient and accurate method of obtaining the local volume-average temperature at each FTT measured position.

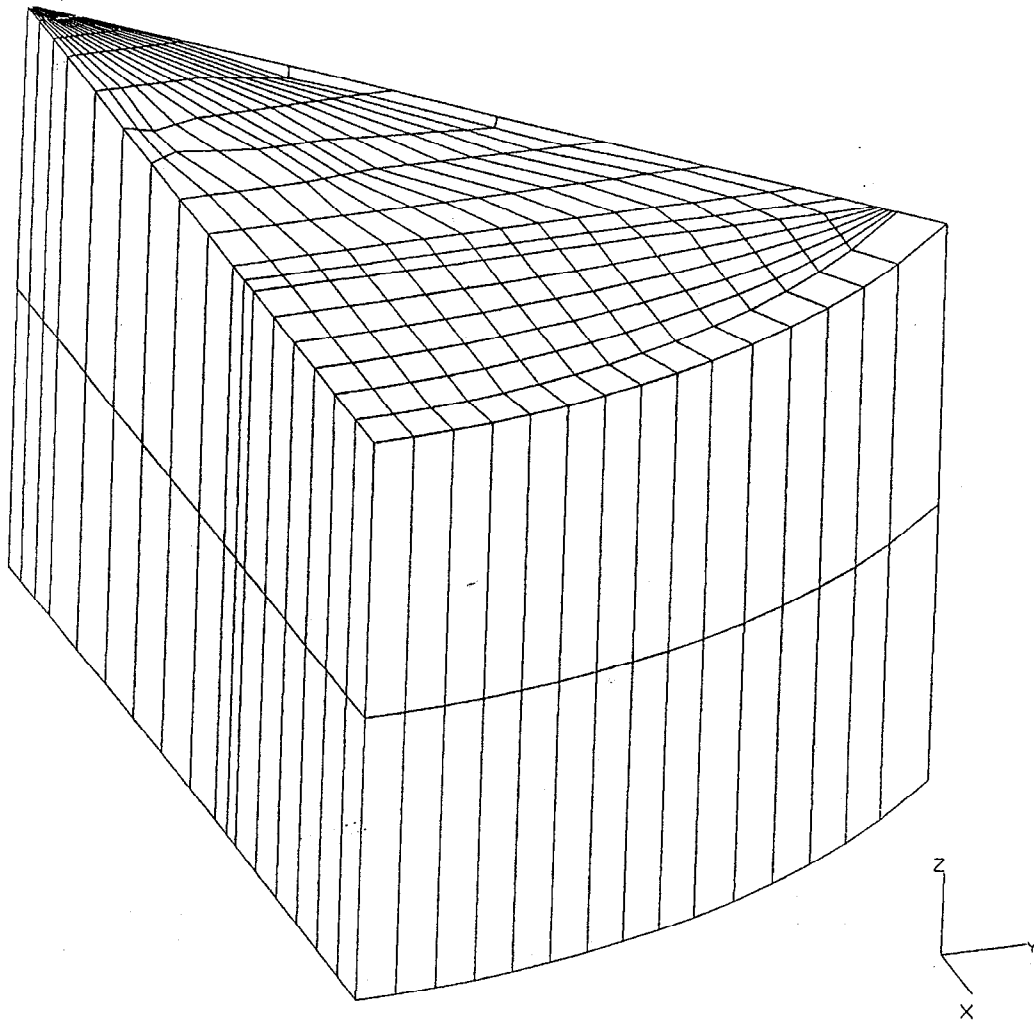


**Figure 10. Perspective view of the TOPAZ3D thermal model of the FTT geometry with the fuel assembly replaced by a solid square log looking towards the center line**

Ingrid/TOPAZ3D: 3-D Simple Model of FTT: SBH31 (4/1) 7.1.95

ENGRID display

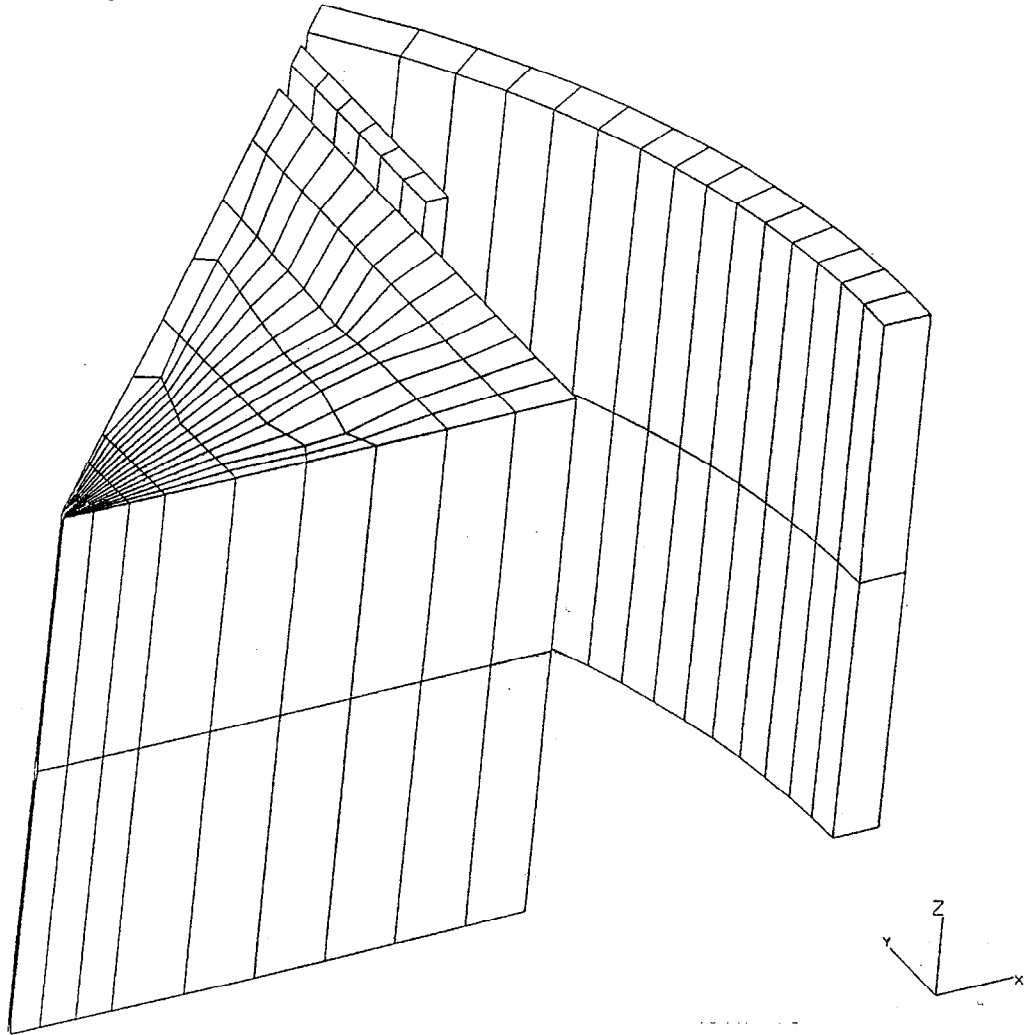


**Figure 11. Perspective view of the TOPAZ3D thermal model of the FTT geometry with the fuel assembly replaced by a solid square log with outer gas region removed looking radially outward**

Ingrid/TOPAZ3D: 3-D Simple Model of FTT: SBH31 (4/1) 7.1.95  
INGRID display

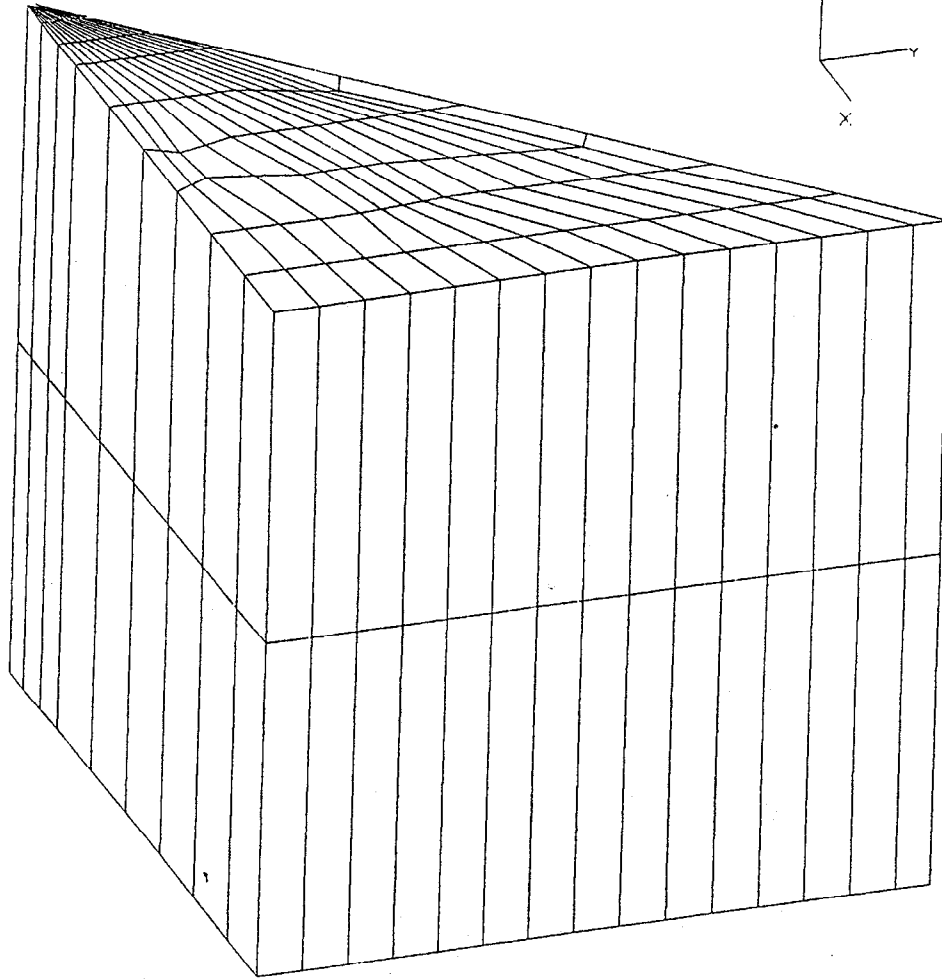


**Figure 12. Perspective view of the solid log looking towards the centerline**

INGRID display

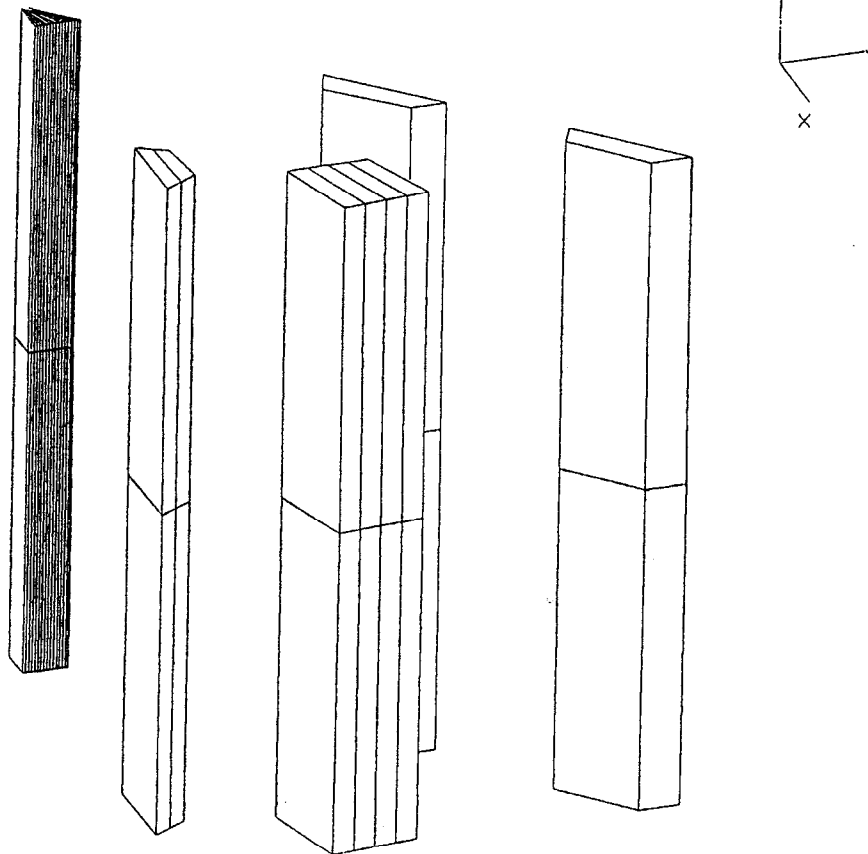


**Figure 13. Perspective view of the five internal vertical regions in the solid square log which represent the FTT temperature locations looking towards the centerline**

The initial solid-log thermal conductivities used in modeling the helium-filled and air-filled cases were representative of typical gases. The initial thermal conductivities for both the solid log and the open gas region outside the solid log were used as a starting point. A separate multiplier was applied to each of these initial values in an iterative fashion to obtain the optimum TOPAZ3D code solutions for each test (helium and air) and for each of the seven axial TC levels. As noted above, varying the multiplier in the open gas region outside the solid log was a simple and effective way of simulating the convective heat transfer portion of the thermal coupling of the solid log to its surroundings.

The angle bracket and the canister wall were both made from stainless steel; their temperature-dependent properties were obtained from Incropera (1985).

As discussed in the previous subsection, the MONT3D code was used to generate the required radiative exchange factor files for all surfaces that can see each other in order to calculate the radiative heat transfer portion of the thermal coupling of the solid log to its surroundings.



## **5.0 RESULTS OF THE SIMULATION OF THE FTT EXPERIMENTS**

### **5.1 Approach to Thermal Modeling of the FTT Experiments**

The Fuel Temperature Test (FTT) experimental series (Bates 1986) that studied heat transfer in a PWR spent fuel assembly, produced a detailed and high-quality data base that is internally self consistent and has well-controlled and characterized boundary conditions. As such, the FTT database is amenable to being simulated using thermal modeling techniques.

The three FTT experiments (vacuum, helium filled, and air filled) involved seven axial levels of 15 TCs each located internal to the spent fuel assembly plus 20 additional TCs mounted on the surrounding temperature-controlled canister wall. The 15 internal TCs at each axial level were symmetrically grouped and averaged into five specific locations across the fuel rod array (Section 3.1.1 and Appendix A). The resulting reduced FTT database used in this study for all three tests is presented in Appendix A.

For each test, the seven axial TC levels were studied in separate thermal analyses (the vacuum test was analyzed at only three axial locations). The criteria for a successful simulation at each axial TC level were:

- 1) closely matching simultaneously all five symmetrically located and averaged-measured temperatures within the fuel rod array using the reported spent fuel assembly total decay heat of 1.17 kW and axial power shape (Figure 9); while
- 2) coincidentally matching the sixth experimental temperature condition of the averaged local canister wall temperature.

In practice, it was found that these criteria could be met with agreement typically to within less than 1°C at all five locations in the fuel rod array. The sixth condition, matching the local canister wall temperature, was an imposed boundary condition in the thermal models.

### **5.2 Thermal Modeling of the FTT Experiments at Vacuum Conditions**

As discussed in Section 4.2, the TOPAZ3D code thermal model represented the vacuum test experimental cross section out to and including both the angle bracket from the Fuel Assembly Support Cage and the canister wall (essentially reproducing the experimental cross section seen in Figure 8).

As discussed in Section 3.3.4, the experimental results for the canister wall showed little azimuthal variation in temperature at any measured axial location. Therefore, throughout this study, the canister wall was treated as an isothermal boundary with the temperature set to the appropriate value for each axial level in each of the three FTT experiments.

The main objective of studying the FTT vacuum experiment was to investigate the ability to model the FTT apparatus in this clean (from a heat transfer view) radiative heat transfer-dominated environment. This objective was successful with analyses at three axial levels producing calculated temperatures that matched the five measured fuel rod array locations to within an average of 2°C, with a maximum deviation of 4.2°C.

The results of the vacuum test analyses indicated that the FTT database could be simulated by thermal modeling and could be used for the solid log concept study. In addition, the iterative process used in converging on the emissivity for the vacuum test analysis indicated that an effective emissivity value of 0.33, a reasonable value for stainless steel (Incropera 1985), could be used for the canister wall in any further FTT thermal modeling.

### 5.3 Thermal Modeling of the FTT Experiments with Helium and Air Conditions

After the vacuum test study, the TOPAZ3D code thermal model was modified. The gas-filled region between the solid log replacement for the fuel assembly and both the angle bracket and the canister wall, was filled with an imaginary material as discussed in Section 4.2.2. The initial thermal conductivity of this material was based on either helium or air, as appropriate for the test, and was changed iteratively in attaining the final TOPAZ3D results discussed in Section 5.4.

As noted in Section 5.2, the five instrumented positions in the FTT fuel assembly were specifically set up with a nodal structure to retain correct position and volume. As a result, the TOPAZ3D code output directly produced the local volume-weighted average temperature for each TC location. It was this set of five calculated temperatures — which, in all cases, were responding to the sixth experimental temperature condition imposed by the canister wall — that were compared to the actual data for temperatures within the FTT spent fuel assembly.

As a result of using this solid log thermal model, it was possible to match all five measurements at six of seven axial locations in both the helium-filled test and in the air-filled test. Some of the possible reasons for not matching the seventh top-most level is discussed in Section 5.4. On the average, these matches were within less than 1°C, with 51 out of 60 possible positions (28 of 30 for helium and 23 of 30 for air) falling in this less-than-1°C category.

Fitting to data involved:

- 1) varying the heat transfer potential external to the log by changing the single-valued thermal conductivity of the gas component in the combined conductive-radiative heat transfer from the surface of the log to the FTT test support stand and the canister wall (the method used to simulate local convective heat transfer); and
- 2) varying the single-valued thermal conductivity of the solid log representing the fuel rods.

Three pairs of example results are presented in Figures 17 to 19. In these figures, the FTT and TOPAZ3D-calculated temperatures for both the helium-filled and air-filled cases are presented for the diagonal plane running from the spent fuel assembly center line through the corner of the assembly. The temperatures continue from the corner of the assembly out through the angle bracket to the canister wall (the left-hand edge of Figure 12). (Please note that the curves connecting the TOPAZ3D results in these figures are smooth fits to the plotted points and represent local temperature gradients only approximately.)

Changing the gas thermal conductivity external to the log established the effective solid-log surface temperature as it responded to the combination of its internal heating and the FTT apparatus-defined external effective thermal resistances. Attaining the stated variation in TOPAZ3D-calculated temperatures within the solid log, within less than 1 K of the actual FTT data, required less than a  $\pm 10\%$  variation in single-valued thermal conductivity for all six helium axial levels and less than  $\pm 20\%$  for all six air axial levels (for levels 3 through 5, see Figures 14 through 16).

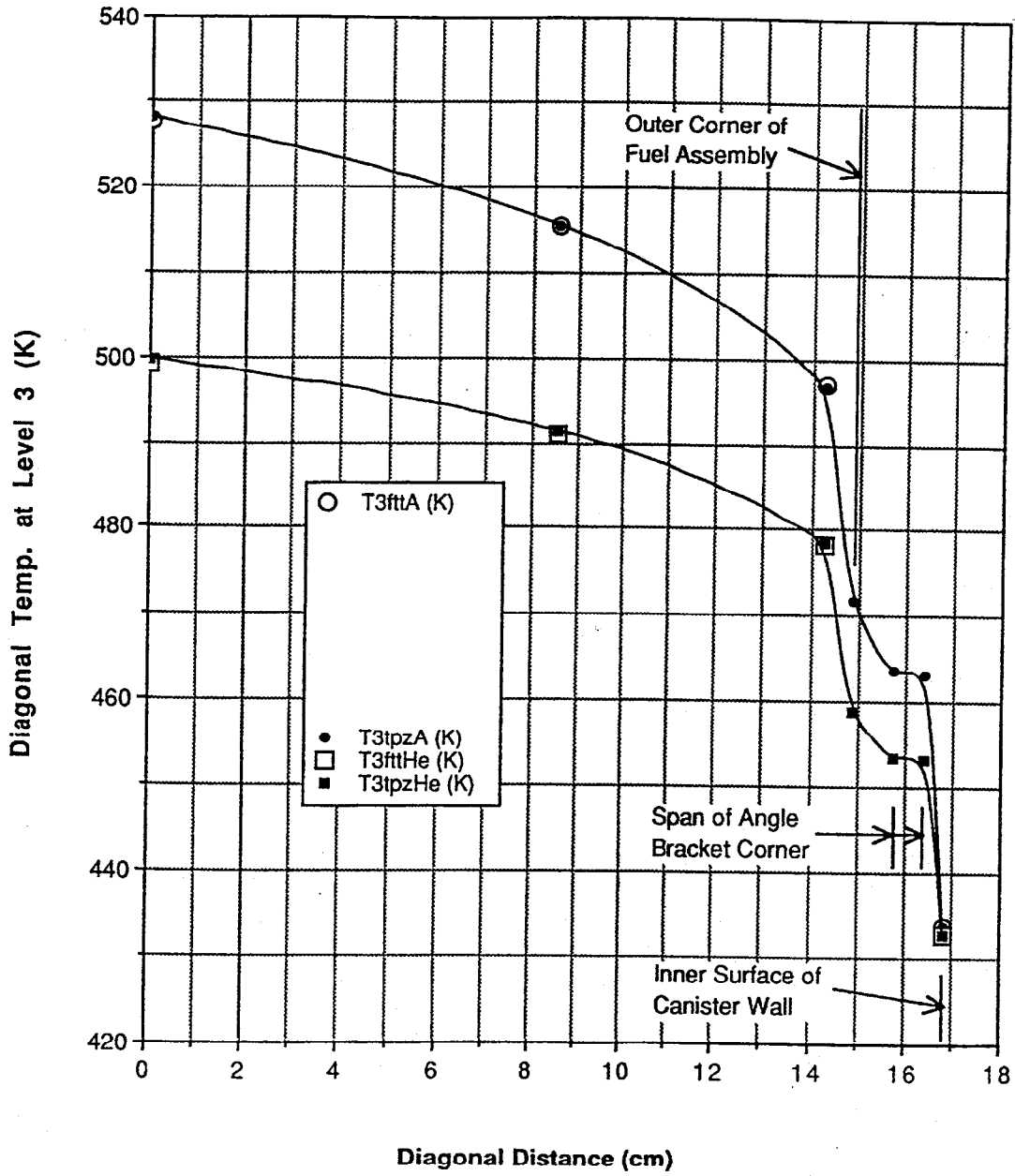


Figure 14. TOPAZ3D versus actual FTT data: helium and air test diagonal temperature distributions at TC level 3

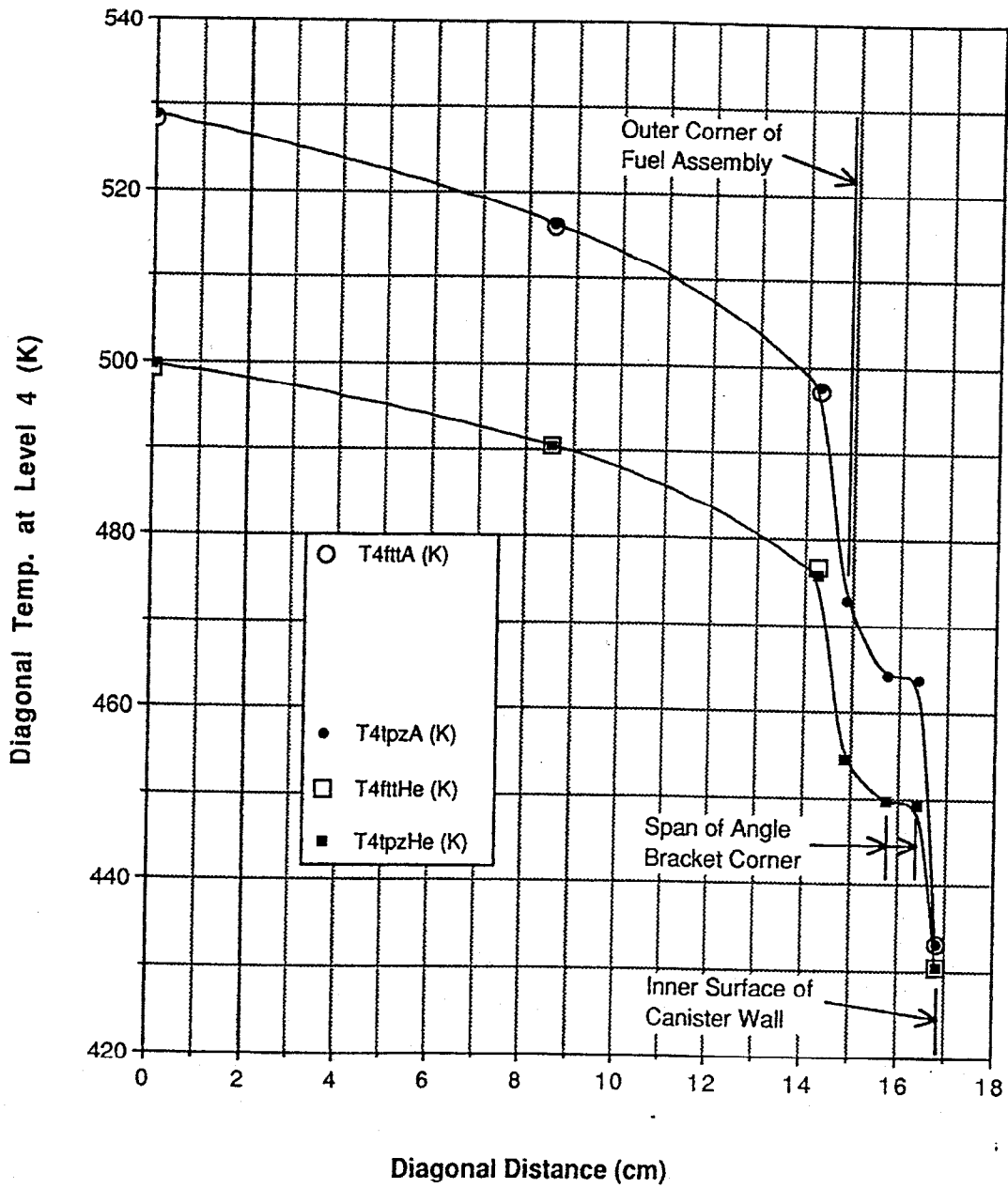


Figure 15. TOPAZ3D versus actual FTT data: helium and air test diagonal temperature distributions at TC level 4

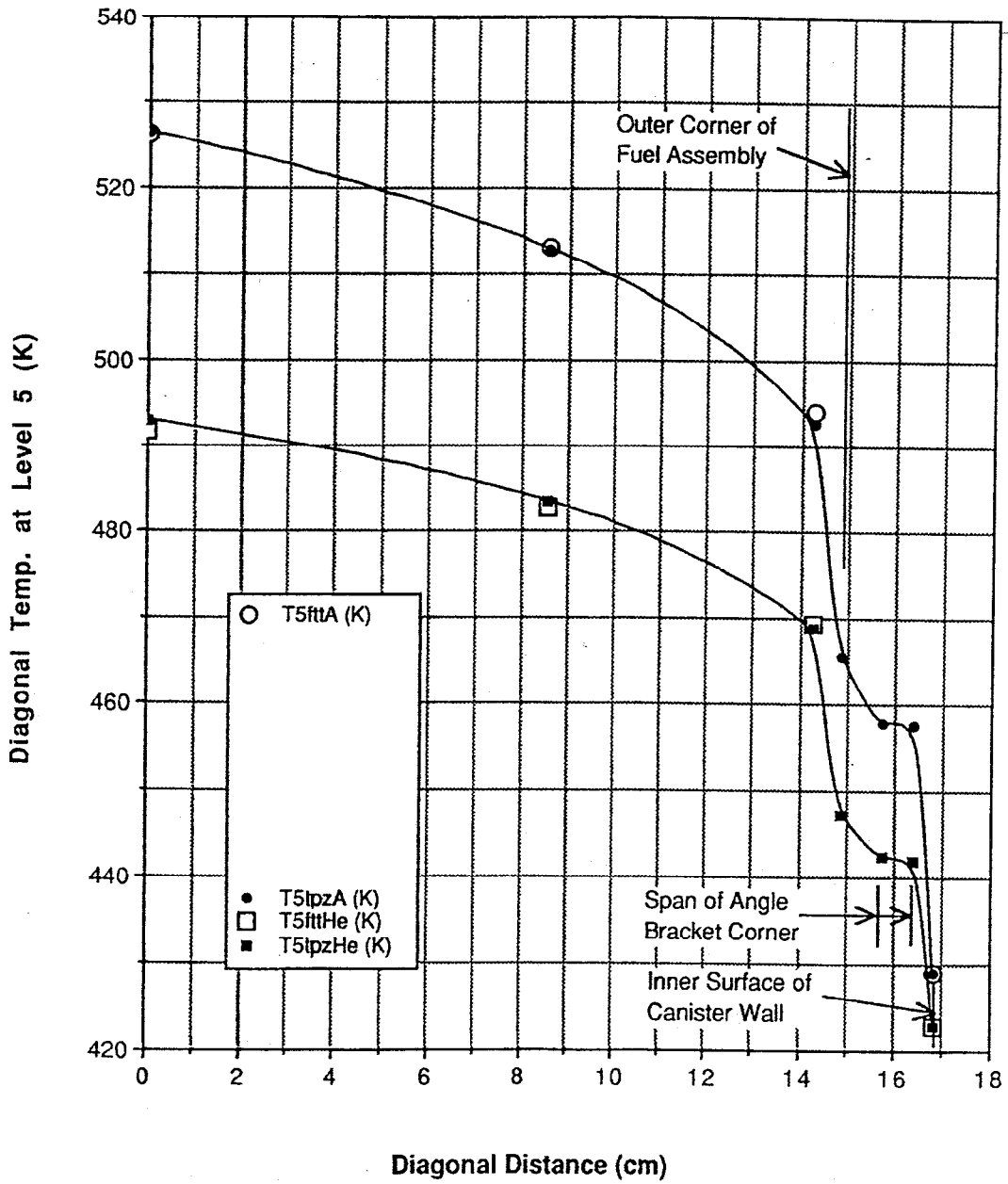


Figure 16. TOPAZ3D versus actual FTT data: helium and air test diagonal temperature distributions at TC level 5

## 5.4 Quantitative Comparison of the FTT Experiments to TOPAZ3D Results

### 5.4.1 Temperature Comparisons

Table 1 shows a summary of the actual comparisons (for all three tests) of FTT-reduced temperature data to the TOPAZ3D-calculated temperatures. This table is oriented with FTT level 7 at the top (as it was in the test). The second column briefly describes each symmetrically located and averaged TC location (Section 3.3.1 and the appendix) at that axial level. The column also includes callouts for the canister wall temperature and the average deviation of the five TOPAZ3D temperatures from the five FTT temperatures.

Under each specific test heading, the first two columns present the FTT and TOPAZ3D temperatures in order, followed by the deviation for each pair (TOPAZ3D minus FTT; the 4.2°C referred to in Section 5.2 for the vacuum test can be found in this column at FTT level 3). The last of the four columns for each test expresses the deviation compared to the overall local FTT temperature drop (measured center line minus canister wall) as a quantitative measure of the difference compared to the temperature driving force in the FTT experiments.

### 5.4.2 Effective Thermal Conductivity Results

A summary of the final effective thermal conductivities resulting from the TOPAZ3D runs and for each level and both the helium-filled and air-filled cases is presented in Table 2. Also included in Table 2 are the average values over level 1 to 6 (see Section 5.4.3 for a level 7 discussion) and the range of these values expressed as a  $\pm$  difference from the reported average value for that gas.

The average single-valued effective thermal conductivity, from Table 2, for the helium-filled and air-filled tests were, respectively, 8.5E-3 watts/cm-°C (0.49 Btu/hr-ft-°F) and 5.8E-3 watts/cm-°C (0.33 Btu/hr-ft-°F). Note that the air value is nearly 70% of the helium value. The helium value has a +4% and -8% range from the average and the air value had a +13% and -22% range from the average.

### 5.4.3 Temperature at Thermocouple Level 7

The calculated versus measured temperatures at TC level 7 did not converge well in the air-filled test (Table 1). In addition, for both tests, notably larger changes in thermal conductivities were required for both the solid log and gap gas and in relatively opposite directions (compared to any of the other six levels) to reach the reported Table 1 conditions. There are several possible causes:

- 1) from Figure 9, level 7 has by far the greatest difference in relative power factor; 0.55 compared to 0.95-to-1.11 for the other six levels and is in a very steep relative power gradient;
- 2) the location of fuel assembly grid spacers is unknown; however, level 7 is close to one of the Fuel Assembly Support Cage horizontal straps.

Because of possible differences in positioning TCs between tests or uncertainty in their position, the relative power factor for level 7 could be much different for each test than the Figure 9 value. In addition, there could be large local errors in the axial power shape in this region. Possibly, the presence of a fuel assembly grid spacer and/or Fuel Assembly Support Cage horizontal strap could affect local convective-conductive-radiative heat transfer, which would be exacerbated by the sharp axial relative power gradient.

Whatever the cause, the level 7 results were sufficiently inconsistent with the other six levels that it was not included in the definition of the average single-valued effective thermal conductivity values reported in Table 2.

**Table 1. Fuel temperature test data compared to TOPAZ3D calculated output**

Fuel Temperature Test Thermocouple Arrangement				Fuel Temperature Test No. 8 Drywell Canister with Vacuum				Fuel Temperature Test No. 7 Drywell Canister with Air				Fuel Temperature Test No. 9 Drywell Canister with Helium			
FIT TC Level/Relative Power Factor	FIT TC Location	Dist. from Bot. of Fuel (in.)	TC Location at Radius (inch)	FIT Ave. Temp (K)	Best Fit Calculated (K)	Difference (Calc.-Data)		FIT Ave. Temp (K)	Best Fit Calculated (K)	Difference (Calc.-Data)		FIT Ave. Temp (K)	Best Fit Calculated (K)	Difference (Calc.-Data)	
						Delta Temp (K)	Total FIT Delta Temp			Delta Temp (K)	Total FIT Delta Temp			Delta Temp (K)	Total FIT Delta Temp
7 0.55	Centerline	140.43	0	452.3				497.0	486.3	-10.7	-13.5%	438.2	437.3	-0.8	-2.3%
	Inner Diagonal		2.38	454.6			488.5	478.8	-7.9	-10.0%	433.5	433.4	-0.1	-0.3%	
	Outer Diagonal		3.97	444.5			471.4	468.2	-3.2	-4.1%	428.3	427.1	0.8	2.0%	
	Mid Row		2.25	453.0			484.4	478.5	-5.9	-7.5%	432.0	433.7	1.7	4.6%	
	Off Set		3.03	451.3			478.7	472.9	-6.8	-8.8%	432.6	430.9	-1.7	-4.4%	
	Canister Wall		7	399.5			417.9	417.6			400.4	400.4			
	Ave. Deviation											-6.9	-8.7%		
6 0.95	Centerline	128.43	0	506.0			521.2	520.1	-1.0	-1.1%	472.7	474.6	2.0	3.2%	
	Inner Diagonal		2.38	497.0			519.8	509.5	-1.3	-1.4%	467.0	467.5	0.5	0.8%	
	Outer Diagonal		3.97	480.8			492.5	484.9	2.4	2.4%	455.8	456.2	0.4	0.6%	
	Mid Row		2.25	497.5			511.4	509.5	-1.9	-1.9%	467.7	468.0	0.3	0.5%	
	Off Set		3.03	480.0			502.8	502.0	-0.8	-0.8%	483.4	483.0	-0.4	-0.7%	
	Canister Wall		7	411.7			423.6	423.6			412.1	412.1			
	Ave. Deviation											-0.5	-0.5%		
5 1.11	Centerline	112.43	0	531.0	534.5	3.5	3.2%	528.2	526.4	0.2	0.2%	491.5	492.8	1.3	1.9%
	Inner Diagonal		2.38	518.6	519.0	1.3	1.3%	513.0	512.9	-0.1	-0.1%	482.8	483.5	0.7	1.0%
	Outer Diagonal		3.97	499.7	500.0	0.3	4.5%	493.9	492.6	-1.3	-1.3%	469.3	468.8	-0.5	-0.8%
	Mid Row		2.25	518.0	520.7	1.7	3.6%	513.2	513.3	0.1	0.2%	483.4	484.1	0.7	1.1%
	Off Set		3.03	509.6	509.2	-0.4	-0.4%	502.9	503.7	0.8	0.9%	477.3	477.6	0.3	0.4%
	Can. Can. Wall		7	422.3	422.3			429.1	429.1			422.8	422.8		
	Ave. Deviation						1.3	2.5%			0.0	0.0%			0.5
4 1.11	Centerline	92.43	0	538.2	538.3	-0.9	-0.6%	528.3	528.7	0.4	0.5%	499.3	499.7	0.4	0.6%
	Inner Diagonal		2.38	528.7	524.0	-2.6	-2.7%	515.9	516.2	0.3	0.3%	490.4	490.4	0.0	0.0%
	Outer Diagonal		3.97	507.5	505.1	-2.4	-1.1%	497.1	497.7	0.6	0.6%	476.6	475.7	-0.9	-1.4%
	Mid Row		2.25	525.9	524.9	-1.0	-0.9%	516.1	516.6	0.5	0.5%	490.8	490.9	0.1	0.1%
	Off Set		3.03	517.3	513.6	-3.7	-3.4%	507.0	507.7	0.7	0.8%	484.8	484.4	-0.4	-0.6%
	Canister Wall		7	429.6	313.7			433.0	433.0			430.5	430.5		
	Ave. Deviation						-2.1	-1.8%			0.5	0.5%			-0.2
3 1.11	Centerline	78.63	0	539.2	539.4	0.2	0.2%	527.5	528.0	0.5	0.5%	499.3	499.7	0.4	0.7%
	Inner Diagonal		2.38	527.4	526.0	-1.4	-1.4%	515.4	515.5	0.1	0.1%	491.1	491.4	0.3	0.5%
	Outer Diagonal		3.97	509.3	506.3	-3.2	0.3%	497.0	496.8	-0.2	-0.2%	478.3	478.4	0.1	0.2%
	Mid Row		2.25	527.8	525.2	-2.6	0.2%	515.7	515.9	0.2	0.2%	491.8	491.9	0.1	0.2%
	Off Set		3.03	519.0	514.8	-4.2	-3.9%	507.5	507.0	-0.5	-0.5%	486.0	486.1	0.1	0.1%
	Canister Wall		7	432.2	316.4			433.9	433.9			433.0	433.0		
	Ave. Deviation						-2.2	-0.9%			0.0	0.0%			0.2
2 1.11	Centerline	52.43	0	536.8			521.0	521.3	0.3	0.3%	496.9	497.4	0.5	0.7%	
	Inner Diagonal		2.38	525.5			519.1	519.3	0.2	0.2%	489.0	489.2	0.2	0.3%	
	Outer Diagonal		3.97	507.3			492.2	484.0	1.8	2.0%	476.1	476.1	0.0	0.0%	
	Mid Row		2.25	528.1			519.6	519.7	0.1	0.2%	489.9	489.7	-0.2	-0.3%	
	Off Set		3.03	517.5			503.0	502.9	-0.1	-0.1%	484.1	483.9	-0.2	-0.3%	
	Canister Wall		7	431.6			431.0	431.0			431.4	431.4			
	Ave. Deviation										0.5	0.5%			0.1
1 1.1	Centerline	30.43	0	527.3			501.3	502.8	1.5	1.8%	486.4	485.6	-0.8	-1.3%	
	Inner Diagonal		2.38	515.5			496.4	490.2	-6.2	-6.2%	477.9	477.4	-0.5	-0.7%	
	Outer Diagonal		3.97	497.2			474.8	470.6	-4.2	-5.2%	464.8	464.2	-0.6	-0.9%	
	Mid Row		2.25	518.1			490.1	490.9	0.8	1.0%	478.3	478.0	-0.3	-0.4%	
	Off Set		3.03	506.3			482.1	482.0	-0.1	-0.1%	472.2	472.2	0.1	0.1%	
	Canister Wall		7	422.1			420.5	420.5			421.4	421.4			
	Ave. Deviation											-0.4	-0.5%		

**Table 2. Comparison of effective thermal conductivities for the best fit from TOPAZ3D runs for each of the seven thermocouple levels in both the helium and air FTT experiments**

Helium-filled FTT Experiment				Air-filled FTT Experiment			
FTT Position	kequivalent W/cm-K	kequivalent Btu/hr-ft-°F	keqHe/keqAir	FTT Position	kequivalent W/cm-K	kequivalent Btu/hr-ft-°F	keqAir/keqHe
TC Level 1	8.80E-03	0.508	1.55	TC Level 1	5.68E-03	0.328	0.646
TC Level 2	8.80E-03	0.508	1.36	TC Level 2	6.49E-03	0.375	0.738
TC Level 3	8.80E-03	0.508	1.55	TC Level 3	5.68E-03	0.328	0.646
TC Level 4	7.81E-03	0.451	1.37	TC Level 4	5.68E-03	0.328	0.727
TC Level 5	7.81E-03	0.451	1.48	TC Level 5	5.27E-03	0.305	0.675
TC Level 6	8.80E-03	0.508	1.55	TC Level 6	5.68E-03	0.328	0.646
TC Level 7	9.35E-03	0.540	2.09	TC Level 7	4.46E-03	0.258	0.477
Average kequivalent*	8.47E-03	0.489	1.48	Average kequivalent*	5.75E-03	0.332	0.680
Spread	4% -8%			Spread	13% -22%		
Ratio kaveHe/kaveAir			1.47	Ratio kaveAir/kaveHe			0.68

\* Average over levels 1 through 6

## 5.5 Quantitative Comparison of Results to the Manteufel and Todreas Study

In Section 5.3.2 and Table 2, the average single-valued effective thermal conductivity for the helium-filled and air-filled tests was reported, respectively, as  $8.5E-3$  watts/cm-°C ( $0.49$  Btu/hr-ft-°F) and  $5.8E-3$  watts/cm-°C ( $0.33$  Btu/hr-ft-°F). A recent study by Manteufel and Todreas (Manteufel 1994) analytically evaluated the effective thermal conductivity of spent fuel assemblies of various designs and compared their results to some experiments. It is possible to directly compare the above average single-valued thermal conductivity values to the equivalent conditions in the Manteufel and Todreas study.

The Manteufel and Todreas study separated the thermal coupling of a spent fuel assembly from its local environment, a wall representing a spent fuel assembly cask basket, into internal (essentially the spent fuel assembly) and external thermal resistances. They report their results as these two separate thermal resistances (proportional to the inverse of the effective thermal conductivity) for the various different spent fuel assembly designs and wall temperatures in Table III of their paper.

In the Manteufel and Todreas study (Manteufel 1994), a comparison was made of the average single-valued effective thermal conductivities to the equivalent conditions for the spent fuel assembly internal thermal resistances. A results comparison between the FTT study and the Manteufel and Todreas study was made with the cases of helium and air (compared to the essentially equivalent nitrogen case of the Manteufel and Todreas study) fill gas. The results of each study were very consistent for each fill gas. The FTT canister wall temperature was used to represent the Manteufel and Todreas study wall temperature for the comparison.

The comparison indicated a factor of about 1.5-2.0 added conservatism for helium and about 1.8-2.2 added conservatism for air in the Manteufel and Todreas study. That is, their results produced lower effective thermal conductivities than reported in this study. As a more quantitative measure, the Manteufel and Todreas approach would produce higher fuel assembly centerline temperatures for the same fuel assembly surface temperature. The difference, for the relatively high FTT decay power (1.17-kW), was about 15 to 20 °C for helium and 40 to 45 °C for air.

In the Manteufel and Todreas study, a variable  $Q$  is defined as total spent fuel assembly decay heat power and is directly proportional to the fuel assembly temperature difference. If this value of  $Q$  was corrected by the FTT local relative axial power factors consistent with the FTT axial TC levels (Figure 9), then the groupings were even closer. The spread for helium of about 1.5 to 2.0 noted above is reduced to about 1.65 to 1.9. The spread for air remained about the same, 2.0 to 2.4 versus the earlier 1.8 to 2.2. However, if the more wayward FTT level 7 situation is included in the revised approach, it also falls in line, increasing the spread only to about 1.65 to 2.1 for helium and 1.65 to 2.4 for air. (With the original definition of  $Q$ , level 7 was nearly a factor of 2 out of line.)



## 6.0 CONCLUSIONS

The Fuel Temperature Tests (FTT) experimentally studied heat transfer in a PWR spent fuel assembly providing a detailed and high-quality data base that was internally self consistent and had well controlled and characterized boundary conditions. As such, the FTT data base permits an examination of the suitability of approximating heat transfer across a fuel assembly by representing the fuel assembly as a homogenous solid or "log" with the same effective cross section, homogenized volumetric heat generation rate, and constant thermal conductivity. Use of the solid log concept is predicated on the assumption that an effective thermal conductivity could be selected such that the temperature distribution within the solid log would closely approximate the temperatures measured in the actual spent fuel assembly.

The three FTT experiments (vacuum, helium filled, and air filled) involved seven axial levels with 15 thermocouples at each level located in the guide tubes plus 20 additional thermocouples mounted on the surrounding temperature-controlled canister wall. The 15 internal thermocouples at each axial level were symmetrically grouped into five specific locations across a symmetry section of fuel rod array. For each test, these seven axial levels were studied in separate thermal analyses (the vacuum test was analyzed at only three axial locations).

The experimental results for the canister wall showed little azimuthal variation in temperature at any measured axial location. As a result, throughout this study the canister wall was treated as an isothermal boundary with the temperature set to the appropriate value for each axial level.

Thermal models representing the experimental cross section out to and including the canister wall were prepared for use with the TOPAZ3D code (Shapiro 1984). For the case where the experimental apparatus was evacuated, an iterative process was used to determine an effective emissivity of 0.33 which could be used in further calculations for the canister wall.

For the cases filled with helium and air, gas was added to the region outside the homogenized fuel assembly. The thermal conductivities of the homogenized fuel assembly and gas were varied until it was possible to match all five measured temperatures at six of seven axial locations in both tests. On the average, these matches were within less than 1°C, with 51 out of 60 possible positions (28 of 30 for helium and 23 of 30 for air) falling in this less than 1°C category. The agreement at the seventh top-most axial location was not as good. Some of the possible reasons for not matching the seventh level is discussed in Section 5.3.

The fitting to data involved:

- 1) varying the heat transfer potential external to the log by changing the single-valued thermal conductivity of the gas component in the combined conductive-radiative heat transfer from the surface of the log to the FTT test support stand and the canister wall (the TOPAZ3D code does not fully model convective heat transfer, but it can be locally simulated in this manner); and
- 2) varying the single-valued thermal conductivity of the solid log representing the fuel rods.

Changing the gas thermal conductivity external to the log established the effective solid-log surface temperature as it responded to the combination of its internal heating and the FTT apparatus-defined external effective thermal resistance. Attaining the stated variation in TOPAZ3D-calculated temperatures within the solid log, within less than 1°C of the actual FTT data, required less than a  $\pm 10\%$  variation in single-valued thermal conductivity for all six helium axial levels and less than  $\pm 20\%$  for all six air axial levels.

Within the range of experiments, there is little obvious temperature dependence of the effective thermal conductivity. The average single-valued thermal conductivity for the helium test and the air test were, respectively:  $8.5\text{E-}3$  watts/cm- $^{\circ}\text{C}$  (0.49 Btu/hr-ft- $^{\circ}\text{F}$ ) and  $5.8\text{E-}3$  watts/cm- $^{\circ}\text{C}$  (0.33 Btu/hr-ft- $^{\circ}\text{F}$ ). Note that the air value is nearly 70% of the helium value.

A comparison of these average single-valued thermal conductivities to the equivalent conditions in the Manteufel and Todreas study (Manteufel 1994) showed very good consistency of results in direct comparison for both helium and air. This comparison indicated a factor of about 1.5-2.2 additional conservatism in the Manteufel and Todreas study (smaller thermal conductivity) over the results of this study. Thus, the Manteufel and Todreas approach would produce higher fuel rod temperatures (by about 15 to 20 $^{\circ}\text{C}$  for helium and about 40-50 $^{\circ}\text{C}$  for air) at the FTT 1.17-kW decay power. If total spent fuel assembly decay heat power was corrected by the FTT local relative axial power factors consistent with the FTT axial thermocouple levels, then the grouping was even closer.

Based upon the results presented above, the reported effective thermal conductivities can be used with a model that represents the fuel assemblies as a homogenous log to determine the heat transfer across fuel assemblies. The model should also represent separately the metal components of the basket and the gas-filled region between the outside of the fuel assembly and the basket. The model should be used to determine the basket temperature around the hottest fuel assembly. The remainder of the analysis should follow current practice by using the Wooton-Epstein correlation to determine the temperature of the hottest fuel rod within the hottest fuel assembly. This approach will reduce the conservatism within the thermal model; however, the determination of the temperature of the hottest fuel rod will not be altered to retain the benchmarking of that analysis.

## 7.0 REFERENCES

- Bates, J. M. 1986. "Single PWR Spent Fuel Assembly Heat Transfer Data for Computer Code Evaluations," PNL-5571, Pacific Northwest Laboratories, Richland, WA.
- J. D. Maltby and P. Burns. 1993. "User's Manual for "MONTE2D and MONTE3D, Monte Carlo Radiative Exchange Factor Codes," Department of Mechanical Engineering, Colorado State University, Fort Collins, CO, UCRL-MA-112192 for Lawrence Livermore National Laboratory.
- Churchill, S. W., and H. H. S. Chu. 1975. "Correlating Equations for Laminar and Turbulent Free Convection from a Vertical Plate," *Int. J. Heat Mass Transfer*, Vol. 18, pp.1323-1329.
- Creer, J. M., et al. 1986. "The Castor-V/21 Spent-Fuel Storage Cask: Testing and Analysis," NP-4887, Electric Power Research Institute, Palo Alto, CA.
- Creer, J. M., et al. 1987. "The TN-24P Spent-Fuel Storage Cask: Testing and Analysis," NP-5128, Electric Power Research Institute, Palo Alto, CA.
- Cuta, J. M and J. M. Creer. 1986. "Comparisons of COBRA-SAS Calculations With Data from Simulated Sections of Unconsolidated and Consolidated BWR Spent-Fuel," NP-4593, Electric Power Research Institute, Palo Alto, CA.
- Incropera, Frank P. and David P. DeWitt. 1985. *Fundamentals of Heat and Mass Transfer*, 2<sup>nd</sup> edition, John Wiley & Sons, New York.
- Masche, George. 1971. "Systems Summary of a Westinghouse Pressurized Water Reactor Nuclear Power Plant," Westinghouse Electric Corporation, PWR Systems Division, Pittsburgh, PA.
- Manteufel, R. D. and N. E. Todreas. 1994. "Effective Thermal Conductivity and Edge Configuration Model for Spent Fuel Assembly, *Nuclear Technology*, Vol. 105, pp. 421 to 440, March.
- McKinnon, M. A., et al. 1987. "The MC- 10 PWR Spent-Fuel Storage Cask: Testing and Analysis," NP-5268, Electric Power Research Institute, Palo Alto, CA.
- McKinnon, M. A., et al. 1989. "Testing and Analysis of the TN-24P Spent-Fuel Storage Cask Loaded with Consolidated Fuel," NP-6191, Electric Power Research Institute, Palo Alto, CA.
- Sparrow, E. M. and J. L. Gregg. 1956. "Laminar Free Convection Heat Transfer from the Outer Surface of a Vertical Cylinder," *Trans. ASME*, **78**, pg. 1823.
- Stillman, D. W. and J. O. Hallquist. 1985. "INGRID: A Three-Dimensional Mesh Generator for Modeling Nonlinear Systems," UCID-20506, Lawrence Livermore national Laboratory, Livermore, CA.







TC Symmetry	TC Level	TC No.	Below Top of Canister (In.)	From Bottom of Fuel (In.)	Radius (Inch)	Orientation (Degrees)	FTT TC Location	Temp (°F)	Temp (K)	Ave. Temp (°F)	Centerline Delta Temp (°F)	Ave. Temp (K)	Temp (°F)	Temp (K)	Ave. Temp (°F)	Centerline Delta Temp (°F)	Ave. Temp (K)	Temp (°F)	Temp (K)	Ave. Temp (°F)	Centerline Delta Temp (°F)	Ave. Temp (K)	Temp (°F)	Temp (K)	Ave. Temp (°F)	Centerline Delta Temp (°F)	Ave. Temp (K)			
1	2	302	113.0	52.43	0	0	Center Line	508.8	536.82	506.80		536.82	478.2	521.04	478.20		521.04	434.8	496.93	434.80		496.93	434.8	496.93	434.80		496.93			
2		344			2.38	45	Inner Diag	489.2	527.15	486.25	20.35	525.51	453.7	507.43	458.48	19.73	510.08	422.4	490.04	420.55	14.25	488.26	419.2	488.26	419.2	488.26	419.2	488.26		
3		365			2.38	225	Outer Diag	484.0	524.26				465.5	513.98																
4		323			3.97	45		455.0	508.15	453.45	53.15	507.29	420.8	489.04	426.30	51.90	492.21	397.5	476.21	397.28	37.53	476.87	398.7	476.87	398.7	476.87	398.7	476.87		
5		386			3.97	225	Mid Row	453.9	507.54				438.2	498.82																
6		372			2.38	135		485.1	524.87				455.1	508.21																
7		330			2.38	315		486.7	525.76				459.6	510.71																
8		400			3.97	135	Off Set	451.4	506.15				421.2	489.37																
9		309			3.97	315		453.5	507.32				425.2	491.59																
10		337			2.25	0		488.7	526.87	487.30	19.30	526.09	456.2	508.82	459.33	18.88	510.55	423.2	490.48	422.13	12.68	489.89	420.1	488.76	420.1	488.76	420.1	488.76		
11		379			2.25	180	Can Wall	484.7	524.65				463.5	512.87																
12		358			2.25	90		488.4	526.71				450.3	505.54																
13		351			2.25	270		487.4	526.15				467.3	514.98																
14		316			3.03	22.5	Off Set	473.8	518.59	471.80	34.80	517.48	439.1	499.32	445.75	32.45	503.01	413.0	484.82	411.70	23.10	484.09	410.4	483.37	410.4	483.37	410.4	483.37		
15		393			3.03	202.5		469.8	516.37				452.4	506.71																
20	Can Wall	431	120.0	45.43	7	0		318.2	431.04	314.45		429.80	313.3	429.43	312.36			315.7	430.76	313.45		429.28	313.45	429.28	313.45	429.28				
21		433			7	180		312.7	429.09				311.4	428.37						311.2	428.26			311.2	428.26					
22		432			7	90		315.9	430.87	313.50				312.6	429.04	311.45				315.3	430.54			315.3	430.54					
23		434			7	270		311.1	428.21					310.3	427.76					309.9	427.54			309.9	427.54					
1	1	301	135.0	30.43	0	0	Center Line	489.8	527.32	489.50		527.32	442.7	501.32	442.70		501.32	415.9	486.43	415.90		486.43	415.9	486.43	415.90		486.43			
2		343			2.38	45	Inner Diag	469.3	516.09	488.20	21.30	515.48	421.9	489.76	423.00	19.70	490.37	401.0	478.15	400.50	15.40	477.87	399.9	477.87	399.9	477.87				
3		364			2.38	225	Outer Diag	467.2	514.93				424.1	490.98																
4		322			3.97	45		437.5	498.43	435.25	54.25	497.18	395.5	475.09	395.00	47.70	474.82	378.5	465.65	377.00	38.90	464.82	399.9	477.54	399.9	477.54				
5		385			3.97	225	Mid Row	432.2	495.48				393.6	474.04																
6		371			2.38	135		467.1	514.87				420.7	489.09																
7		329			2.38	315		469.2	516.04				425.3	491.65																
8		399			3.97	135	Off Set	434.3	496.65				393.8	474.15																
9		308			3.97	315		437.0	498.15				397.1	476.98																
10		336			2.25	0		471.4	517.26	472.90	16.60	518.09	425.0	491.48	422.55	20.15	490.12	403.2	479.37	401.25	14.65	478.29	399.9	477.54	399.9	477.54				
11		378			2.25	180	Can Wall	466.6	514.04				421.3	489.43																
12		357			2.25	90		468.1	515.43				418.0	487.69																
13		350			2.25	270		486.5	525.65				425.9	491.98																
14		315			3.03	22.5	Off Set	455.0	508.15	451.65	37.85	506.29	410.4	483.37	408.05	34.65	482.07	392.1	473.21	390.20	25.70	472.15	401.5	478.43	401.5	478.43				
15		392			3.03	202.5		448.3	504.43				405.7	480.76																
22	Can Wall	435	154.5	10.93	7	90		263.4	401.71	261.95		400.90	263.6	401.82	262.05			265.2	402.71	263.75		401.90	263.75	401.90						
23		436			7	270		260.5	400.09				260.5	400.09						262.3	401.09			262.3	401.09					

**Table A-2: FUEL TEMPERATURE PRIMARY DATA REDUCTION**

TC Level	Below Top of Canister (In.)	From Bottom of Fuel (In.)	Radius (Inch)	FTT TC Location	FUEL TEMPERATURE TEST NO. 8 TEST CONDITIONS: Drywell Canister with Vacuum			FUEL TEMPERATURE TEST NO. 7 TEST CONDITIONS: Drywell Canister with Air			FUEL TEMPERATURE TEST NO. 9 TEST CONDITIONS: Drywell Canister with Helium		
					Ave. Temp (°F)	Centerline Delta Temp (°F)	Ave. Temp (K)	Ave. Temp (°F)	Centerline Delta Temp (°F)	Ave. Temp (K)	Ave. Temp (°F)	Centerline Delta Temp (°F)	Ave. Temp (K)
Can Wall	16.5	148.93	7		238.50		387.87	281.80			241.70		389.65
7	25.0	140.43	0	Center Line	372.50		462.32	435.00		497.04	329.00		438.15
			2.38	Inner Diag	359.10	13.40	454.87	416.08	18.93	486.53	320.65	8.35	433.51
			3.97	Outer Diag	340.45	32.05	444.51	388.93	46.08	471.44	307.75	21.25	426.34
			2.25	Mid Row	355.80	16.70	453.04	412.33	22.68	484.44	317.88	11.13	431.97
			3.03	Off Set	352.70	19.80	451.32	403.80	31.20	479.71	318.95	10.05	432.57
			7	Can Wall	259.49	113.01	399.54	291.97	143.03	417.58	261.06	67.94	400.40
6	37.0	128.43	0	Center Line	451.20		506.04	478.40		521.15	391.10		472.65
			2.38	Inner Diag	434.98	16.23	497.03	459.80	18.60	510.82	380.95	10.15	467.01
			3.97	Outer Diag	405.80	45.40	480.82	426.90	51.50	492.54	360.83	30.28	455.83
			2.25	Mid Row	435.88	15.33	497.53	460.83	17.58	511.39	382.20	8.90	467.71
			3.03	Off Set	422.35	28.85	490.01	445.05	33.35	502.62	374.45	16.65	463.40
			7	Can Wall	281.38	169.82	411.70	302.87	175.53	423.63	282.12	108.98	412.11
Can Wall	51.0	114.43	7		298.60	197.50	421.21	312.20	175.30		299.55	125.45	421.73
5	53.0	112.43	0	Center Line	496.10		530.98	487.50		528.21	425.00		491.48
			2.38	Inner Diag	473.83	22.27	518.61	463.70	23.80	512.98	409.37	15.63	482.80
			3.97	Outer Diag	439.78	56.33	499.69	429.28	58.23	493.86	385.13	39.88	469.33
			2.25	Mid Row	474.50	21.60	518.98	464.00	23.50	513.15	410.38	14.63	483.36
			3.03	Off Set	457.60	38.50	509.59	445.50	42.00	502.87	399.50	25.50	477.32
			7	Can Wall	300.39	195.71	422.25	312.72	174.78	429.11	301.40	123.60	422.82

TC Level	Below Top of Canister (In.)	From Bottom of Fuel (In.)	Radius (Inch)	FTT TC Location	Ave. Temp (°F)	Centerline Delta Temp (°F)	Ave. Temp (K)	Ave. Temp (°F)	Centerline Delta Temp (°F)	Ave. Temp (K)	Ave. Temp (°F)	Centerline Delta Temp (°F)	Ave. Temp (K)
4	73.0	92.43	0	Center Line	510.80		539.15	491.20		528.26	439.00		499.26
			2.38	Inner Diag	488.30	22.50	526.65	468.98	22.23	515.91	423.10	15.90	490.43
			3.97	Outer Diag	453.85	56.95	507.51	435.13	56.08	497.11	398.28	40.73	476.64
			2.25	Mid Row	487.03	23.78	525.94	469.33	21.88	516.11	423.85	15.15	490.84
			3.03	Off Set	471.50	39.30	517.32	452.85	38.35	506.96	413.05	25.95	484.84
			7	Can Wall	313.70	197.10	429.65	319.64	171.56	432.95	315.29	123.71	430.53
Can Wall	85.5	79.93	7		316.70	194.20	432.07	320.30	169.60		319.00	120.00	432.87
3	86.8	78.63	0	Center Line	510.90		539.21	489.90		527.54	439.00		499.26
			2.38	Inner Diag	489.58	21.33	527.36	468.10	21.80	515.43	424.25	14.75	491.07
			3.97	Outer Diag	457.35	53.55	509.46	434.93	54.98	497.00	401.20	37.80	478.26
			2.25	Mid Row	490.45	20.45	527.84	468.68	21.23	515.75	425.53	13.48	491.78
			3.03	Off Set	474.50	36.40	518.98	453.75	36.15	507.46	415.20	23.80	486.04
			7	Can Wall	318.35	192.55	432.23	321.40	168.50	433.93	319.75	119.25	433.01
2	113.0	52.43	0	Center Line	506.60		536.82	478.20		521.04	434.80		496.93
			2.38	Inner Diag	486.25	20.35	525.51	458.48	19.73	510.08	420.55	14.25	489.01
			3.97	Outer Diag	453.45	53.15	507.29	426.30	51.90	492.21	397.28	37.53	476.08
			2.25	Mid Row	487.30	19.30	526.09	459.33	18.88	510.55	422.13	12.68	489.89
			3.03	Off Set	471.80	34.80	517.48	445.75	32.45	503.01	411.70	23.10	484.09
			7	Can Wall	317.29	189.31	431.64	316.05	162.15	430.96	316.87	117.93	431.41
Can Wall	120.0	46.43	7		314.45		429.80	312.35			313.45		429.28
1	135.0	30.43	0	Center Line	489.50		527.32	442.70		501.32	415.90		486.43
			2.38	Inner Diag	468.20	21.30	515.48	423.00	19.70	490.37	400.50	15.40	477.87
			3.97	Outer Diag	435.25	54.25	497.18	395.00	47.70	474.82	377.00	38.90	464.82
			2.25	Mid Row	472.90	16.60	518.09	422.55	20.15	490.12	401.25	14.65	478.29
			3.03	Off Set	451.65	37.85	506.29	408.05	34.65	482.07	390.20	25.70	472.15
			7	Can Wall	300.14	189.36	422.12	297.24	145.46	420.50	298.79	117.11	421.37
Can Wall	154.5	10.93	7		261.95		400.90	262.05			263.75		401.90